



**National  
Oceanography  
Centre**

# **USING OPTICAL SATELLITE SHORELINE DETECTION TO MEASURE HISTORIC AND FORECAST FUTURE SANDY SHORELINE CHANGES IN NORTH AFRICA**

Report - Version 1.0. August 2020

**Submitted by** Stephen Carpenter, with input from Miguel Toquica (WBG) and Christine Sams

**In Cooperation with:**



**THE WORLD BANK**

This report was produced by the National Oceanography Centre as part of the World Bank MENA Blue Program North Africa Blue Economy and Coastal Management - (P170596) and Integrated marine and coastal management in Tunisia - (P166339) technical assistance. The study was funded by the ESA EO4SD Marine and Coastal initiative. EO4SD is a 3-year project supporting large scale application of EO as a key source of globally consistent environmental data to support the development and delivery of international development activities

## Contents

Executive Summary	3
1. Introduction	5
1.1. Objectives	5
1.2. Drivers of Shoreline Change	6
1.3. Availability and Limitations of Existing Data	6
2. Overview of Methodology	7
2.1. Limitations	8
3. Results and discussion	10
3.1. Tunisia	13
3.1. Morocco	16
3.2. Soliman Beach Case Study - Coastal Infrastructure Effects for Erosion protection	18
4. Recommendations	24
5. References	25
Annex A: Detailed Description of Methodology	29
Annex B Shoreline Change Rates / Admin Level 2 (Governorate/Province)	39

## Executive Summary

This report shows the findings of a study on coastline changes in the Middle East and North Africa Region. This exploratory study has been conducted in response to a request for large scale coastline change mapping at higher resolution than currently openly available. The results provide a 'best available' dataset which is unvalidated (i.e. no ground truthing of the results has been carried out), and is limited to sandy (or soft) coastlines and aspects associated with the underlying data such as the difficulties in mapping complex and low-lying coastlines and cross-satellite change analysis. These are described in detail within the report. It is critical to note that EO is most effectively used in combination with in-situ data and local knowledge, and recommendations are made to validate the results presented.

This study exploits the processing power of Google Earth Engine to download annual median composites to map shoreline change by using open-sourced tools such as *Coastsat* (Vos et al., 2019a) and the Digital Shoreline Analysis System (DSAS) (Himmelstoss et al., 2018). Shorelines are delineated using yearly Landsat 7, 8 and Sentinel 2 images from 2000 to 2020 and a baseline is extracted to cast transects at 50m intervals along the coast. Shoreline change statistics are calculated using intersects with the shorelines and transects and a linear forecast using historical rates to predict future shorelines to visualise the impact at 10- and 20-year intervals.

The key findings from this report include:

- Results indicate overall accretion of 0.15 and 0.03m/yr in Mediterranean coast Morocco and Tunisia, respectively. In contrast to Atlantic coast Morocco and Western Sahara which are eroding at -0.09 and -0.45m/yr, respectively.
- Accretion is occurring along 36%, 28%, 28% and 34% of the Morocco (Mediterranean), Morocco (Atlantic), Western Sahara and Tunisia coasts respectively. Of these figures, 5.9%, 3.2%, 2.6% and 3.8% represents severe or extreme accretion. In the next decade, accretion of approximately 5.2, 3.0, 3.8 and 7.4km<sup>2</sup> are indicated for Morocco (Atlantic), Morocco (Mediterranean), Western Sahara and Tunisia, respectively. This assumes no intervention and is based on an extrapolation of historic rates.
- Erosion is occurring across 37%, 39%, 37% and 35% of Morocco (Mediterranean), Morocco (Atlantic), Western Sahara and Tunisia respectively. Of these figures, 1.4%, 1.3%, 3.2% and 4.5% is severe or extreme erosion. In the next decade erosion of approximately 8.5, 1.9, 11.2 and 7.1km<sup>2</sup> is expected for Morocco (Atlantic), Morocco (Mediterranean), Western Sahara and Tunisia, respectively. As above this assumes no intervention and is based on extrapolation of historic rates.

## Glossary and abbreviations

Acronym/abbreviation	Text in full
<b>B</b>	Blue
<b>DSAS</b>	Digital Shoreline Analysis System
<b>EO</b>	Earth Observation
<b>EO4SD</b>	Earth Observation for Sustainable Development (ESA funded initiative)
<b>ESA</b>	European Space Agency
<b>ETM</b>	Enhanced Thematic Mapper
<b>FES2014</b>	Finite Element Solution tide model 2014
<b>G</b>	Green
<b>GEE</b>	Google Earth Engine
<b>MNDWI</b>	Modified Normalized Difference Water Index
<b>MSI</b>	Multi-Spectral Instrument
<b>NIR</b>	NIR Near-Infrared
<b>OLI</b>	Operational Land Imager
<b>PSMSL</b>	Permanent Service for Mean Sea Level
<b>R</b>	Red
<b>SAR</b>	Synthetic Aperture Radar
<b>SLC</b>	Single Look Complex Processing Level
<b>SPOT</b>	Satellite Pour l'Observation de la Terre
<b>SWIR</b>	Shortwave Infrared
<b>TM</b>	Thematic Mapper
<b>TOA</b>	Top-of-Atmosphere
<b>UNESCO</b>	United Nations Educational, Scientific and Cultural Organization
<b>USGS</b>	United States Geological Survey
<b>WBG</b>	World Bank Group

## 1. Introduction

This short study has been conducted by NOC within the framework of the ESA-funded EO4SD Marine and Coastal Resources project. It seeks to address a knowledge gap in the availability of national, country scale statistics on rates of coastal change (accretion and erosion) for the North African coastline. Specifically, this study improves on previous work through the use of higher resolution data (e.g. Luijendijk et al. 2018). The study focuses on the full length of the coastlines of Morocco and Tunisia, considering change over the period from 2000 to 2020.

### 1.1. Objectives

The objectives of this project are to explore rates of shoreline change (erosion and accretion) and make predictions on the area lost or gained across Tunisia and Morocco (Figure 1); a coastline over 2900km in length (approximately 1150km and 2500km respectively). Due to the extent of Morocco's coastline, the country was split into two parts, northern Morocco, herein referred to as Morocco, and Western Sahara.

A workflow has been developed and documented using optical satellite image processing to map historical changes in the physical location of annual median shoreline positions, plotting transects at 50m intervals. Analysis of the historic rates of change at these locations has then be used to give an approximate projection of future change, assuming all other factors remain constant. Details of the methodology and associated limitations are included in Annex A.

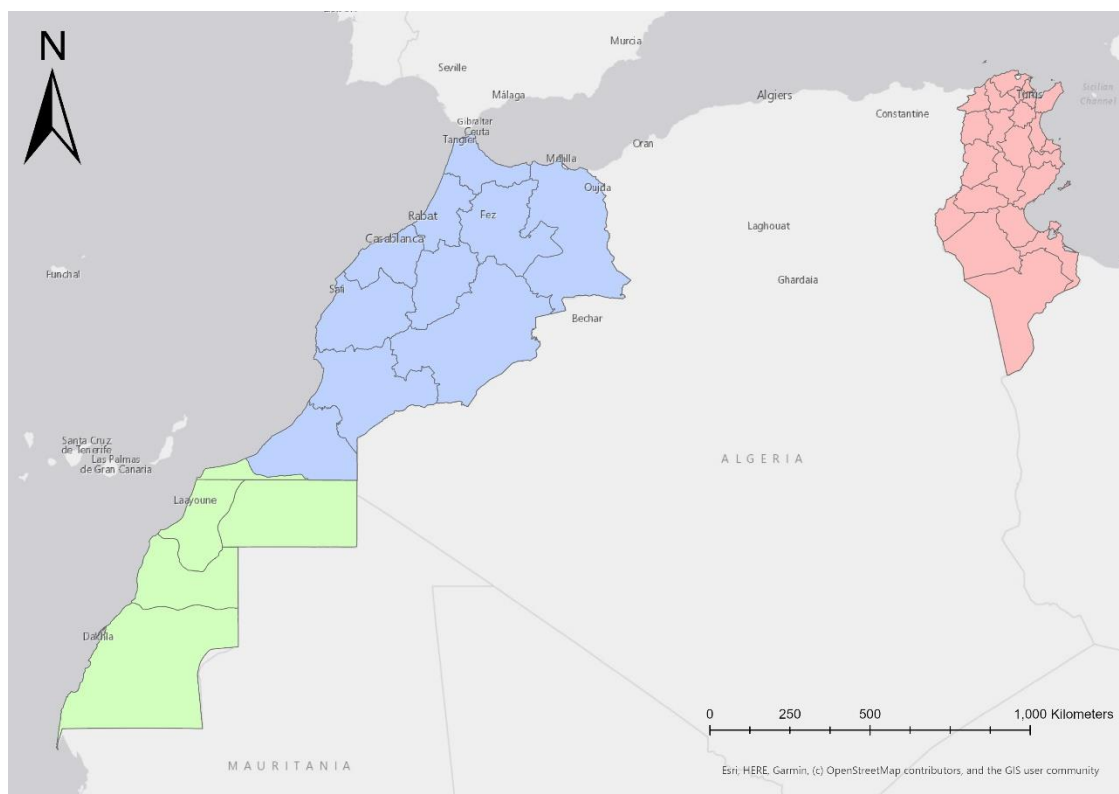


Figure 1. Morocco split into north (blue) and Western Sahara (Green) and Tunisia (red).

It is intended that work will be extended to produce results across the remaining countries in North Africa (Algeria, Libya and Egypt), this was not possible within the timeframe of this initial study. The simplicity of the workflow is essential in enabling its integration in the capacity development activities of EO4SD and shared amongst the wider scientific community of Northern Africa and elsewhere.

It is important to note that results presented in this report have not been validated against in-situ data or local expertise and therefore should be treated as preliminary only.

## 1.2. Drivers of Shoreline Change

There are a number of factors that drive coastline change, these are often divided into human-induced factors (coastal subsistence, defence developments, tourism infrastructure or land reclamation) and natural physical forcing elements (e.g. storm events, sea-level rise, sediment transport) (Sytnik et al., 2018). Coastal areas with different tidal dynamics and wave energy indices demonstrate unique coastal morphologies (Hayes and FitzGerald, 2013). Fluvial and alongshore sediment transport are major morphodynamic processes which determine the shape of the coastline (Sytnik et al., 2018) and often dictate how the coast is managed through division into sediment cells. Human interventions, such as ports or groynes, intervene in the hydrodynamic processes along the shoreline. Often, they stabilise areas by sediment build up in one location, but cause sediment starvation and intensification of erosion rate further along the shoreline.

North African countries are especially at risk as they lie within the transitional zone between subtropical temperate and continental climates that are exposed to more severe forecasted climate change effects (Amrouni et al., 2019). Increasing ocean temperatures causing thermal expansion is one of the main drivers of global sea-level rise, which is projected to increase by 50-98 cm by 2100 (IPCC, 2014).

Rapid growth in urban coastal populations increases pressure on coastal systems. In the Naubel governorate and Hergla community in Tunisia coastal populations increased up to 47% between 1984 and 2014 (Tunisian National Institute of Statistics, 2014). Population growth brings development leading to changes to the natural environments and habitats that provide natural protection such as wetland 'sabkha' (Ayache et al., 2009, Kouzana et al., 2010, Zghibi et al., 2011, Chekirbane et al., 2013, Amrouni et al., 2019).

## 1.3. Availability and Limitations of Existing Data

Presently, the literature on shoreline change in North Africa is limited to specific beaches or zones or global studies of shoreline change. The most recent country-scale analysis was carried out by Luijendijk et al. (2018); this compiled yearly composites of satellite images dating from 1984-2016 and computed transects at 500m intervals globally<sup>1</sup>. In this dataset, erosion and accretion are calculated based on a threshold between water and sandy beaches. As reported by Pardo-Pascual et al. (2018), white-water caused by waves

---

<sup>1</sup> The results from this analysis are available in the form of an online web map (<https://aqua-monitor.appspot.com/?datasets=shoreline>).

breaking as they approach the shore, is one of the largest sources of error in shoreline classifications. This issue is not highlighted by Luijendijk et al. (2018), but has been compensated for in this study through its separate classification and removal before delineating the shoreline.

The approach adopted in this study seeks to improve the precision and accuracy of the Luijendijk et al. (2018) dataset by:

1. Increasing resolution from 500m to 50m transects
2. Performing analysis using higher resolution images (restricting the satellites to those launched from the year 2000 onwards means all have a resolution of <15m when using the panchromatic band)
3. Modifying the processing workflow to reduce the errors arising from white-water miss-classification

## 2. Overview of Methodology

As indicated, this study utilises satellite remote sensing techniques (optical data processing) to facilitate large-scale rapid geospatial analysis. Previously, understanding of shoreline dynamics was limited to photogrammetry or in-situ measurement. Satellites have greatly enhanced the ability to measure coastal change over large areas and at short intervals. This has transformed monitoring capabilities and should be seen as complementary to in-situ assessments, rather than a direct replacement of conventional mapping techniques.

The methodology follows seven key stages:

1. The download of annual median composites of Landsat 7, 8 and Sentinel 2 images from Google Earth Engine
2. Co-registration of Landsat images to Sentinel 2
3. Pre-processing of the data (cloud masking and pansharpening<sup>2</sup>)
4. Image Classification
  - a. Normalised Difference Water Index
  - b. Supervised classification of images into Sand, Land, White-water and Water classes
5. Shoreline Delineation using Otsu's thresholding (Otsu, 1979) and marching squares algorithms
6. Casting Transects
7. Calculating change rate statistics
8. Forecasting

---

<sup>2</sup> Pansharpening is a process of lowering the resolution of a multispectral image using a higher-resolution panchromatic band

A full description of each step is given in Annex A. Annual median composites were used instead of individual satellite images to minimise the impact of tides<sup>3</sup>. There are no tide gauge data available for Morocco and Tunisia according to the Global Sea Level Observing System (GLOSS | The Global Sea Level Observing System, 2021) to enable correction for tides. Nevertheless, even supposing a chain of tide gauges, the inherent complexity of tidal differences along the coastline make correcting for tide extremely difficult over large areas.

## 2.1. Limitations

The use of EO for coastline change monitoring has specific limitations that must be considered when applying the results.

Firstly, the advantage of median composites relies greatly on the number of images available from each satellite for each shoreline. Image availability is determined by the revisit time of satellites; cloud cover; the location of the study area on the Earth; and whether the study area is within an overlapping region along a satellite's flight path. For Landsat 5 and 7, the overlap between adjacent orbits is nearly 84% at extreme latitudes, compared 7.3% at the equator (The Worldwide Reference System, 2020). For example, in this study the number of cloud minimal images in Morocco ranged from a single tile, up to 434 tiles per region. The scan line error which occurred on Landsat 7 31<sup>st</sup> May 2003, combined with the longer revisit time means fewer images are available. The availability of a large number of images becomes common in later years with Sentinel 2 as there is data available from two satellites (2A and 2B) that together have a 5-day revisit frequency. In this study, the mean number of images used in the median composites for each satellite were 16, 25 and 94 images for Landsat 7, Landsat 8 and Sentinel 2, with a standard deviation of 9, 12 and 68, respectively. A reduced number of images used in the median can result in the presence of cloud in the final composite and may fail to resolve seasonal and interannual variability sufficiently. This can have an ongoing and detrimental effect on the shoreline output where cloud halos can result in shorelines delineated by the algorithm. In cases where shorelines have been derived from a small number of images, they may be skewed by the impact of tides, especially when these images are concentrated within a particular time of year. Future iterations of this analysis could include Landsat 5 data (which was not included due to python scripting difficulties that could not be resolved in the available time-period) to increase the number of images available in earlier years. Additionally, setting a lower cloud threshold to remove images with a high cloud presence would reduce the possibility of artefacts in the median image.

A second limitation occurs when transects are cast in river inlets they may be drawn between land surfaces (e.g. a single transect between both side of a split), these must be removed to prevent false change. Similarly, shorelines delineated in low-lying, intertidal areas are too distant from each other for transects to

---

<sup>3</sup> Tides change on a daily and monthly basis. Satellites capture a single snapshot in time in a given area. Therefore, performing change analysis using individual dates even on the same day of the year and at a similar time of day can result in a vastly different coastline position.



be cast (see Annex A, Limitations for further details), as a result the shoreline change rate in these areas is not represented. The complex nature of low-lying intertidal areas makes it difficult to capture a change rate over time in these areas, which cannot be represented sufficiently using a median composite. A more thorough editing process, such as the manual drawing of transects, is needed to ensure they intersect with the correct shoreline. The large scale of this study and the time restrictions meant that transects along complex coastlines or across human structures were not all removed. Therefore, transects can display extreme values of accretion and erosion which may skew the regional and national averages. A more complex analysis of low-lying areas over a transect/intersect methodology is needed, perhaps by finding the mean centre point of all lines for individual years (for more detail see Annex A, Limitations).

Thirdly, despite implementing a co-registration process, there are occasionally differences between shorelines in Landsat and Sentinel-2 images. Whilst local 'rubber sheet' <sup>4</sup>deformations were used to match images from the two satellites, further interrogation of the offset images showed that the offset values greatly depended on the images used in the analysis, i.e. Offset values calculated from the same Landsat slave image using a master Sentinel 2 image from 2016 differed from an equivalent in 2017. The explanation for this difference is unknown at the time of this report, though it is likely to be a result of a difference in the ground control points that would have been identified automatically by the co-registration function in Google Earth Engine. It was deemed suitable to maintain this co-registration process despite occasional improper warping to minimise the difference between Landsat and Sentinel shorelines. A further enquiry into the processes within the Earth Engine functions 'displacement' and 'displace' is needed to understand how this is affecting the co-registration between the images. Satellite mapping of shorelines is generally accurate to 10m (Himmelstoss et al., 2018), this is indicative of the uncertainties in the processing. There are continued efforts to provide a more detailed quantification of the uncertainties within the co-registration process and median composites outside this report.

Finally, the algorithm used has been developed for sandy beaches. Therefore, shoreline change in non-sandy coastlines is not represented in the data. A modification of the classification stage in the workflow, which discriminates a cliff-water boundary over a sand-water interface, is required to understand change in these areas.

### 3. Results and discussion

In order to maintain interoperability between this report and Luijendijk et al. (2018), we adopt a near-identical classification scheme, modified from Esteves and Fink (1998). Here, three higher classes of accretion (shown in blue) are added. Shoreline change rates are classified as:

- Extreme Accretion >5m/yr.
- Severe Accretion 3 to 5m/yr.
- Intensive Accretion 1 to 3m/yr.
- Accretion >0.5m/yr.
- Stable -0.5 to 0.5m/yr.
- Erosion -1 to -0.5m/yr.
- Intense Erosion -3 to -1m/yr.
- Severe Erosion -5 to -3m/yr.
- Extreme Erosion <-5m/yr.

North Morocco statistics are split into Atlantic/Mediterranean at the Ksar es-Seghir port, as it was expected that there may be a difference in the nature of shoreline evolution due to hydrodynamic processes at the coast. Our analysis has shown that coastlines facing the Mediterranean have a lower percentage of sandy coastlines; with Morocco showing 75% and Tunisia 85% (Table 1). Whereas the Atlantic side of Morocco and Western Sahara coastline demonstrating a near-complete sandy composition at 96% and 100% respectively. The high percentage of sandy coastlines in this region demonstrates the appropriateness of this analysis, which is suited to beach areas. Unexpectedly, the aggregated shoreline change rate calculated for the Mediterranean coast of Morocco suggests accretion at an average rate of 0.15m/yr. This is considerably higher than the 2018 study by Luijendijk et al. (2018), which found an overall average erosion rate of -0.14m/yr. Likewise, the Atlantic shoreline change rate is higher in this study at -0.09m/yr. Similarly, this study suggests that Tunisia's shoreline erosion rate is also slower, at -0.25m/yr compared with the Luijendijk et al (2018) calculation of -0.7m/yr. In contrast, the Western Sahara mean change rate has increased, with the results showing an overall rate of erosion of -0.45m/yr., in comparison to the Luijendijk et al (2018) result of -0.09m/yr.

There are several reasons why the results of the current study may differ from the work of Luijendijk et al (2018) with the key differences being the exclusion of white-water; the time-period of analysis; and the resolution of data used. The mean change statistic should be interpreted with caution as it is heavily influenced by outliers, common in areas of significant change such as estuaries or surrounding anthropogenic developments. Nonetheless, the difference in coastline change rates in Morocco from overall erosion to accretion is particularly striking. An increase in erosion rates in Western Sahara when compared to Luijendijk et al. (2018) demonstrates a less anthropogenically influenced case study in an area of lower development - Western Sahara is estimated to have a population of ~600,000 compared to Morocco's ~37 million (United Nations Population Division, 2020). Nevertheless, these statistics provide a national view of local processes, areas of drastic change will be neutralised by the lack of change elsewhere along the coast. To understand the hydrodynamics behind these statistics requires a local view of the change rates, whilst visualising individual yearly shorelines to comprehend how the coast is changing over time.

Table 2. Descriptive and Shoreline Change statistics (Mean across country)

Country	Sandy (%)	Shoreline Count*	Shoreline Change Rate (m/yr.)	Shoreline Change Rate (m/yr.) Luijendijk et al. (2018)
Morocco (Atl)	96	18.1	-0.09	-0.12
Morocco (Med)	75	18.2	0.15	-0.14
Western Sahara	100	16.8	-0.45	-0.09
Tunisia	85	17.8	0.03	-0.70

\*Average Number of shorelines used in the calculation of change rate statistics

The positive rate of shoreline change in Morocco (Mediterranean), Table 1, is responsible for the projected greater accretion than erosion (of >1km<sup>2</sup>) in the first 10 years, Table 2. For Western Sahara, the erosion is projected to be considerable, with a mean shoreline change rate -0.45m/yr, the eroded area is forecast to be almost three times that of the accreted area by 2030. In Tunisia, accretion areas remain similar to erosion with both areas increasing by ~4km<sup>2</sup> between the 10- and 20-year forecast. This suggests that the country will undergo a large shift in material along the coast rather than a gain or loss.

Table 2. Total Change Area under ‘No Active Intervention’ from forecast using historical data. The impact of recent developments in future estimations may not be captured.

Country	Erosion Area 10yrs (km <sup>2</sup> )	Accretion Area 10yrs (km <sup>2</sup> )	Erosion Area 20yrs (km <sup>2</sup> )	Accretion Area 20yrs (km <sup>2</sup> )
Morocco (Atl)	8.55	5.19	13.24	7.12
Morocco (Med)	1.89	2.97	3.54	4.33
Western Sahara	11.15	3.76	17.54	6.47
Tunisia	7.11	7.37	11.03	11.80

A more holistic perspective can be gained by comparing the percentage of areas undergoing different shoreline dynamics (Figure 2). Tunisia illustrates a relatively evenly balanced shoreline change for each category, sediment here is transported along the coast but shifted to a different location. Overall change rates in Mediterranean Morocco are positive (there is greater accretion than erosion) and include a large proportion of severe accretion which is 2% more than severe erosion. Atlantic Morocco is demonstrating overall erosion at around 10% higher than all active accretion along the coast. In Western Sahara, extreme accretion is the single class which outweighs its erosional counterpart.

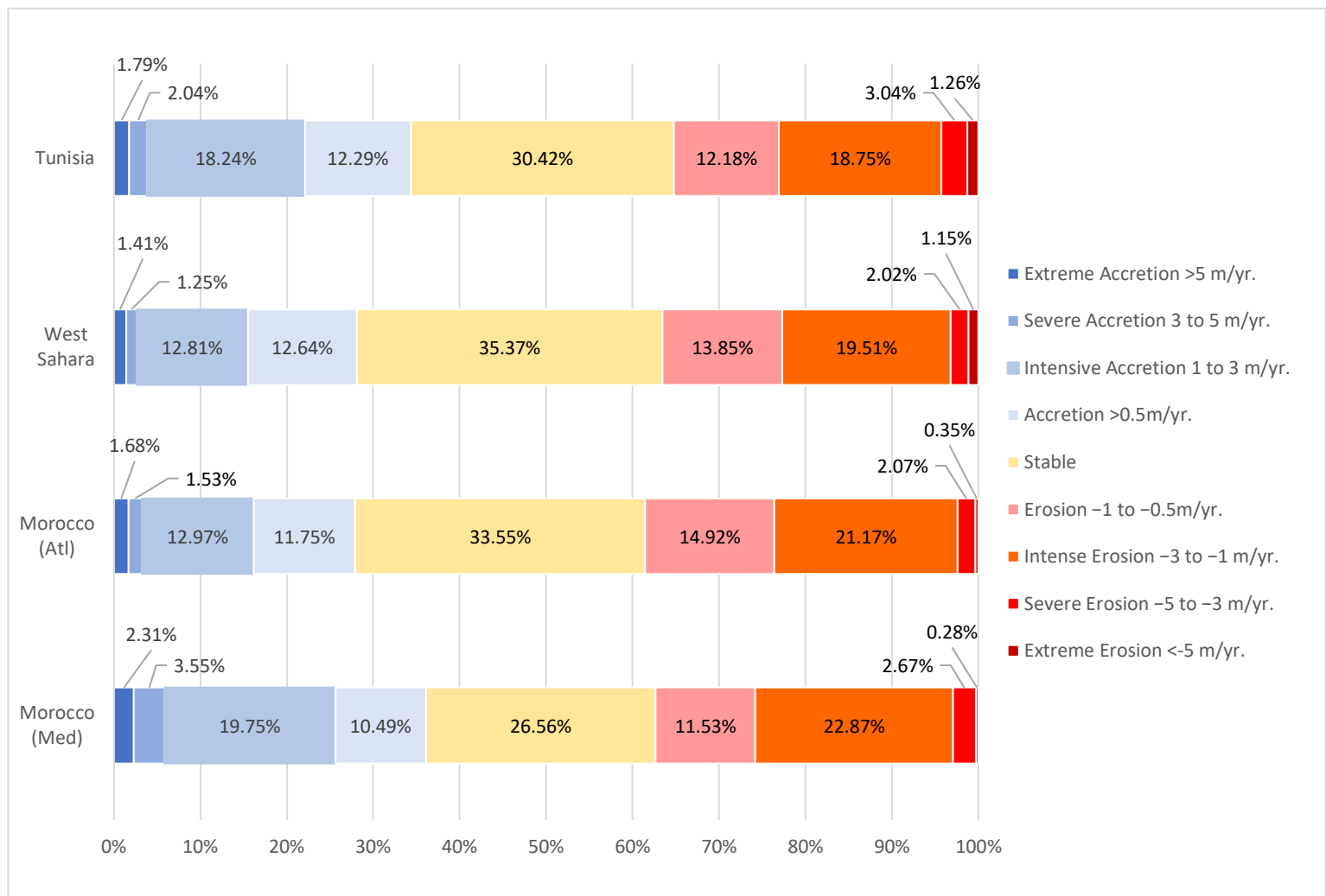


Figure 2 Proportion of accreting, eroding and stable shorelines by country/region.

The following sections provide illustrations of the shoreline change using level-2 administrative boundaries<sup>5</sup>. Figures are presented by aggregating the data to hexagons to better visualise the data. Hexagons represent the shape and direction of the coastline whilst reducing sampling bias (Sahr et al., 2003). After experimentation, a 15km<sup>2</sup> hexagon was deemed suitable for Morocco and 50km<sup>2</sup> for Tunisia, to summarise a mean shoreline change rate over the three areas. A breakdown of regional erosion rates for each country is given in Annex B.

---

<sup>5</sup> Levelled administrative boundaries were developed by the United Nations to enable a consistent GIS dataset worldwide, where level 2 represents the 2<sup>nd</sup> level below the national boundary of a country, often a county, district or province (Home | Second Administrative Level Boundaries, 2021)

### 3.1. Tunisia

Shoreline change in Tunisia is hugely varied (Figures 3 and 4), the highest accreting area is located along the coast of Sfax, Gabes and Medenine, the latter of which frequently demonstrating extreme or severe accretion. Intensive accretion (1-3m/yr) is occurring within a 50km<sup>2</sup> zone in 13 provinces, including Mareth and Medina, both in Gabes (Annex B). Intensive erosion is distributed in seven main areas, including Utique

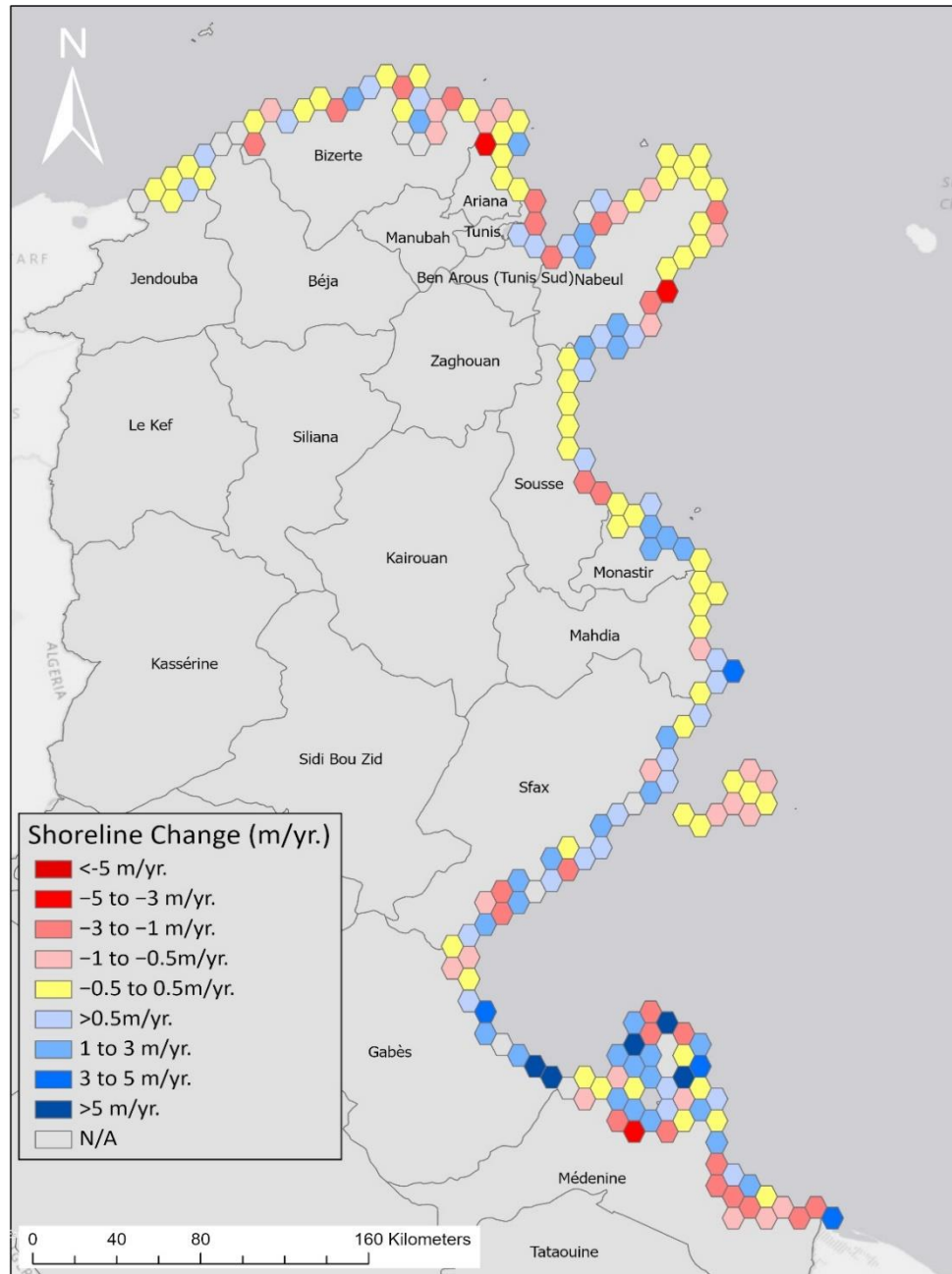


Figure 3. Tunisia Shoreline Change Rates aggregated to 50km<sup>2</sup> hexagons.

in Bizerte and Korba in Nabeul with more 2m/yr. Whilst the state of shoreline change is mixed and therefore stable, there appears to be more erosion occurring in the north, with more accretion in the south.

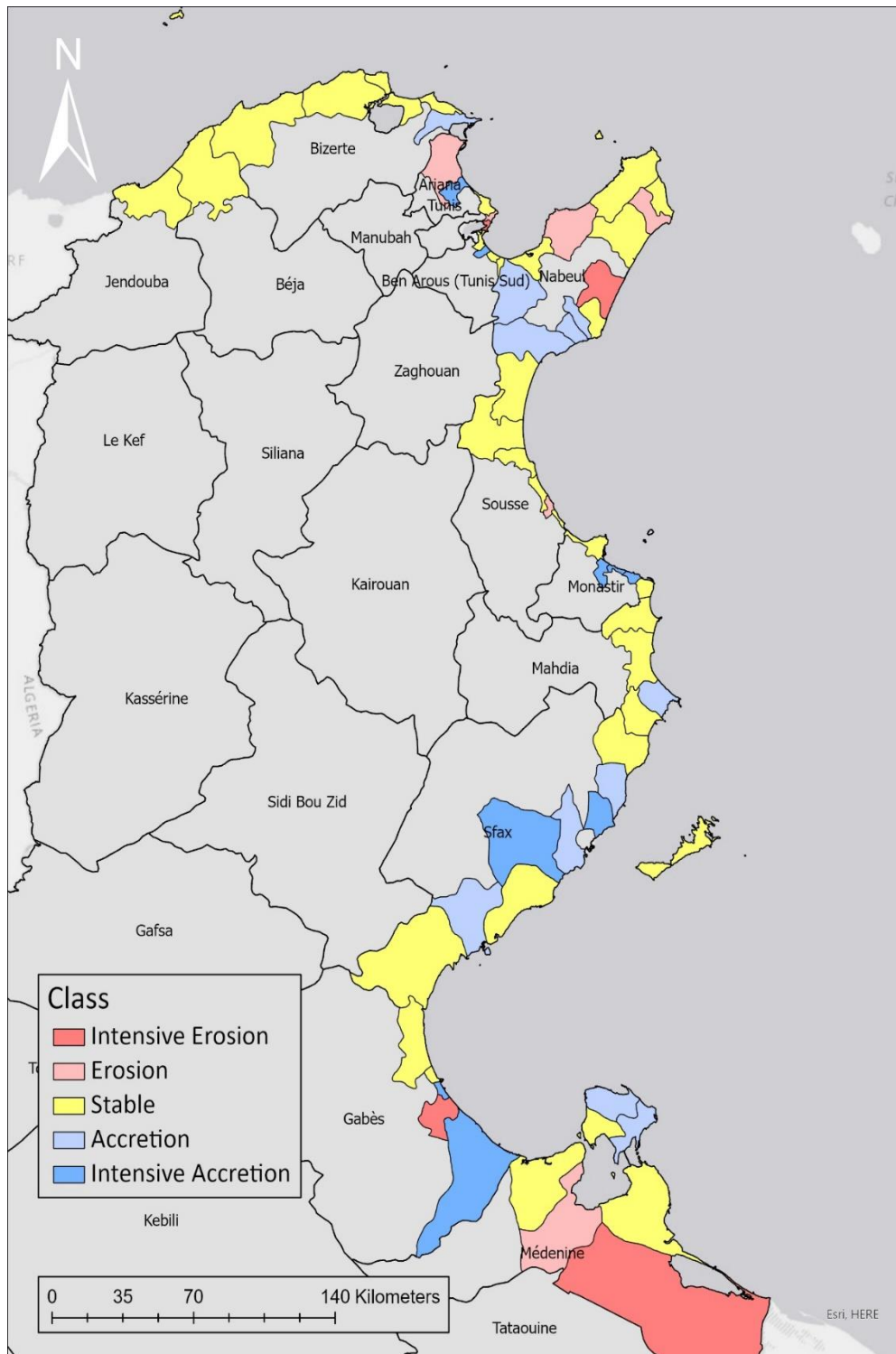


Figure 4. Tunisia Shoreline Change Rates aggregated to Level -2 administrative boundaries

Forecast shoreline positions for a 10- and 20-year period are illustrated below, at a local scale (Figure 5). The lines represent the high-water mark expected based on the previous two decades of shoreline movement, with no adjustment based on local management decisions such as the building of defences or managed realignment. Uncertainty bands are given which match the U.S Geological Survey suggestion that shorelines can be measure within a 95% confidence to within 10m. Two cases are present showing locations which currently experience severe/extreme erosion and severe/extreme accretion.

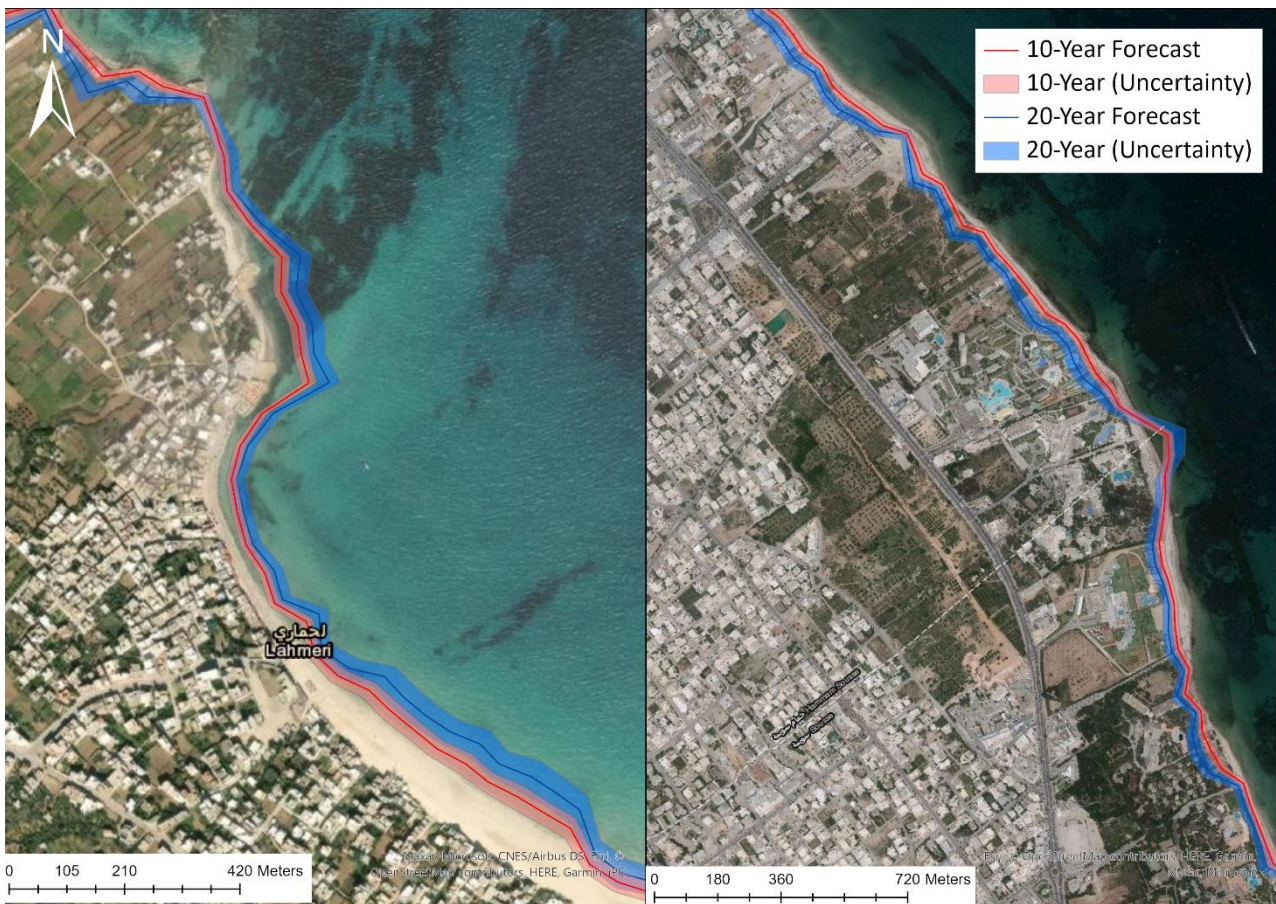


Figure 5. Shoreline change forecast of the mean high-water line. Left = accreting areas in Lahmeri, Tunisia. Right = Eroding areas in Hammam Sousse, Tunisia

### 3.1. Morocco

Along Morocco’s north Atlantic coastline, erosion is common in the Larache (in the North) and El Jadida (in the South) provinces (Figure 6). Intensive erosion is also occurring in regions of Kenitra and Nouaceur, the latter a possible effect of Casablanca’s large port. Pockets of severe or extreme accretion can also be found around the port in Casablanca and the spit at Mohammedia.

Larache is a coastal town and gives its name to the province. Extensive and regular sand mining activity occurs along the coast as sand is a popular commodity used as a critical ingredient to concrete, glass and microchips (Coastal Care, 2020). This may be causing the elevated erosion rates in a region that may otherwise be stable according to its two neighbours; Kentria and Tangier Assilah.

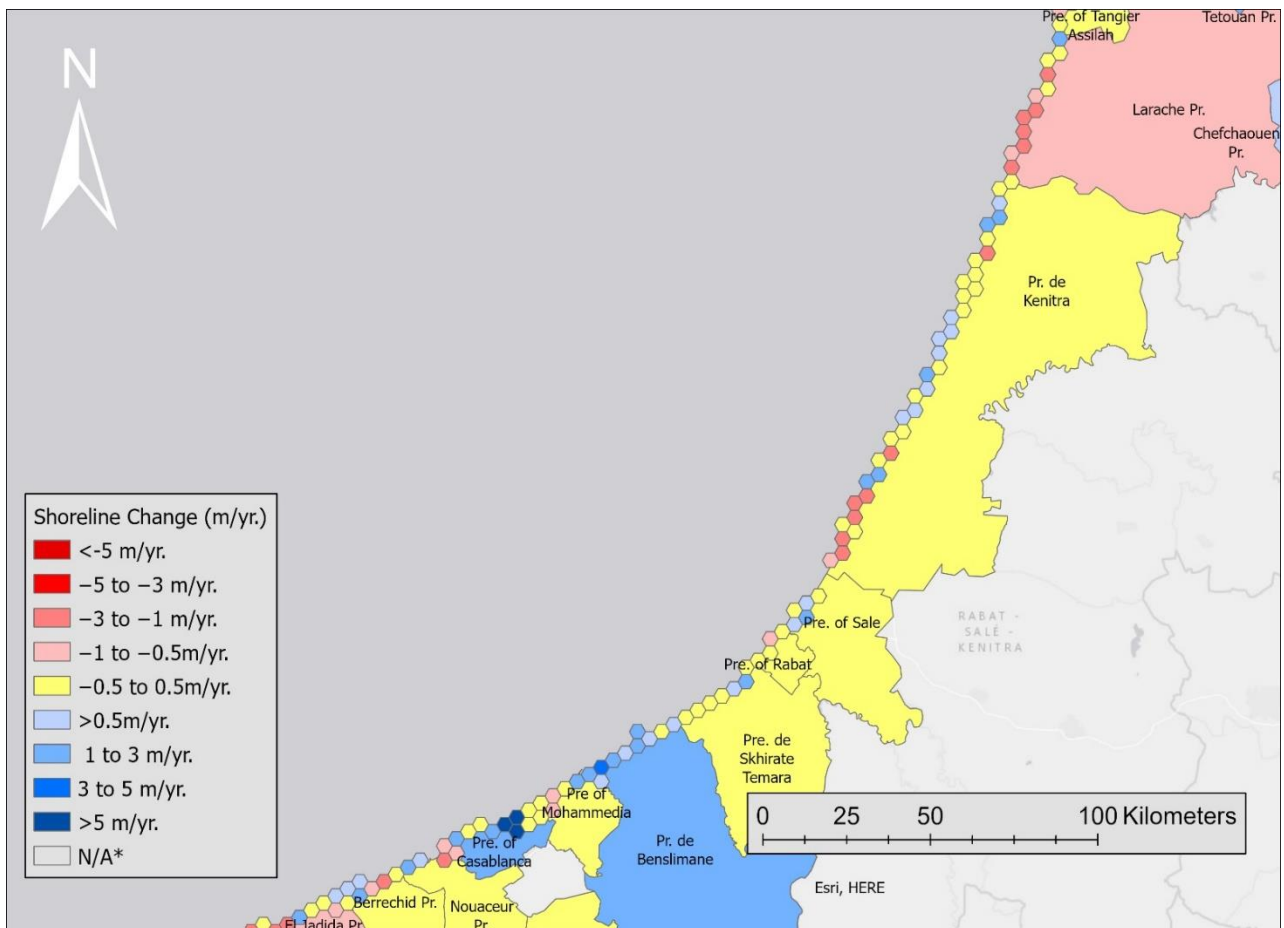


Figure 6 Morocco [Atlantic-side] Shoreline Change Rates aggregated to 15km<sup>2</sup> hexagons. \* N/A due to non-sandy coastline or lack of baseline before 2004. Map includes level-2 admin boundaries classified into mean shoreline change classes. Pre= Prefecture. Pr=Province



On Morocco's Mediterranean coast, intensive accretion is occurring in the Fahs Anjra and Tetouan Provinces (Figure 7). Anthropogenic developments such as one of Africa's largest ports, a 1.6km<sup>2</sup> long port called Tanger-Med on the strait of Gibraltar, are likely to have a significant and potentially ongoing effect on shoreline change rates. A further possible source of change relates to the hydrological cycle and the rates of river flow deposition at estuarine locations. This has not been investigated in this study but these are inherently variable systems, which may experience significant interannual and decadal variability. In spite of this, such a widespread deposition rate seems unlikely since there are numerous studies on the threat of the Moroccan coastline due to sea level rise (Snoussi et al., 2008; Snoussi et al., 2009; Kasmi et al., 2020). Further east along the Mediterranean coast of Morocco, erosional processes become more dominant. The largest sections of erosion are occurring either side of the Driouch Province in the Al Hoceima Bay Port and surrounding the Port Nador West Med. A combination of miss-registration issues and coastal infrastructure developments are resulting in the apparent severe accretion rates within the lagoon at Nador which concretes the need for a complete validation of the shoreline data given in this report. Clusters of intensive

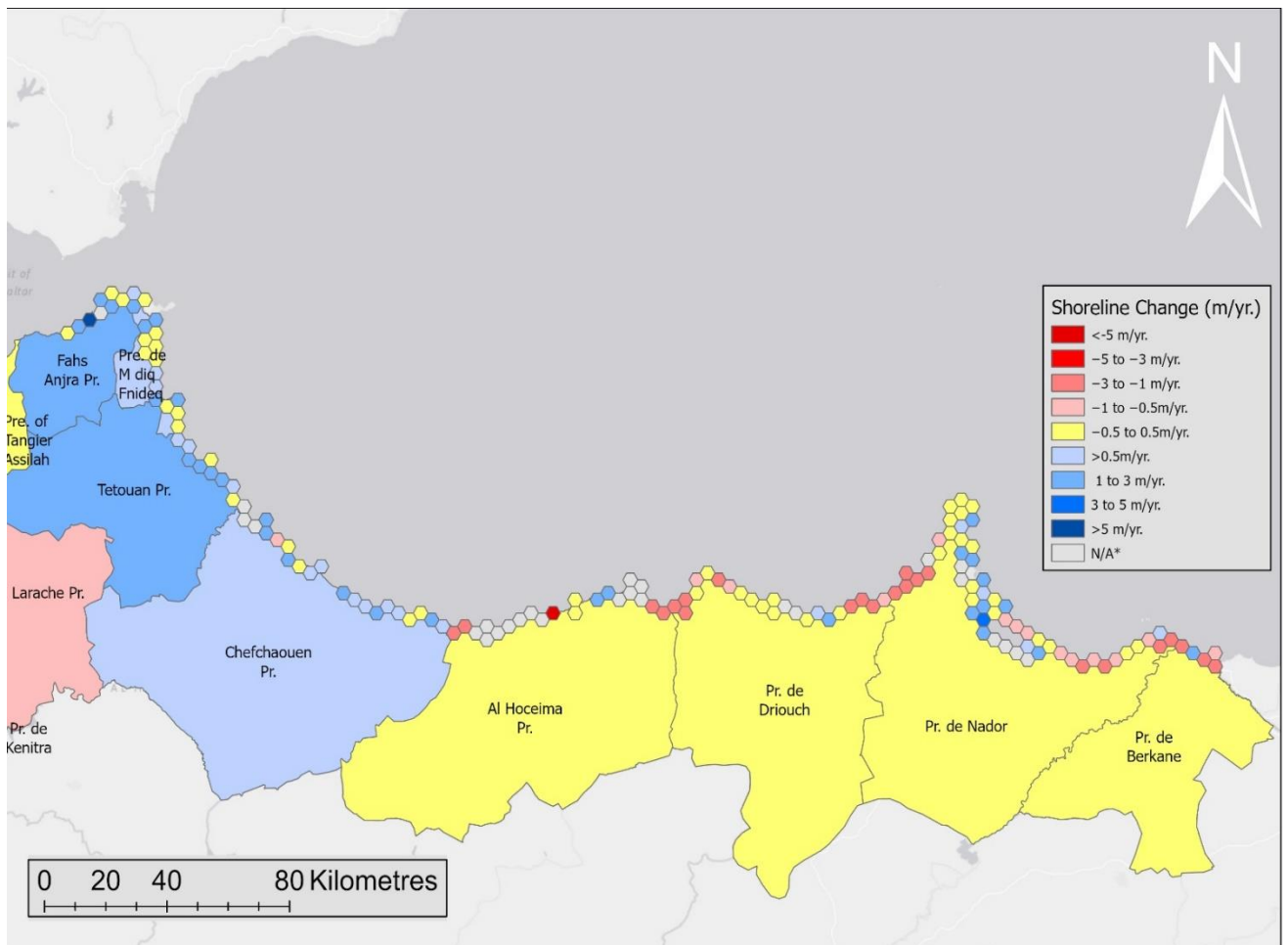


Figure 7. Morocco [Mediterranean-side] Shoreline Change Rates aggregated to 15km<sup>2</sup> hexagons. \* N/A due to non-sandy coastline or lack of baseline before 2004. Map includes level-2 admin boundaries classified into mean shoreline change classes. Pre= Prefecture, Pr=Province

erosion are occurring at the western and eastern coastal boundaries of Nador but, like the rest of the coastline, these have little effect on the variability at the prefecture/provincial scale.

### 3.2. Soliman Beach Case Study - Coastal Infrastructure Effects for Erosion protection

#### Overview

The coastal zone of Soliman is located in the gulf of Tunis, South East of the city of Tunis (Figure 8). This coastline, in particular, has seen strong rates of coastal erosion which have been acted onto protect the natural and urban development through infrastructure projects in the late in 1980s early 1990s. A number of experts have studied the effects of the infrastructure on the sediment movement (erosion vs accretion) (Hanen et al., 2012). Initially, a set of breakwaters were built in 1989 and 1990 for coastal protection, more recently, in 2018, these breakwaters were replaced by coastal groynes. An additional analysis has been carried out using EO tools and analysis to better understand the effects of the breakwaters and the groyne-system on the coastal sediment and erosion patterns of the Soliman beach.

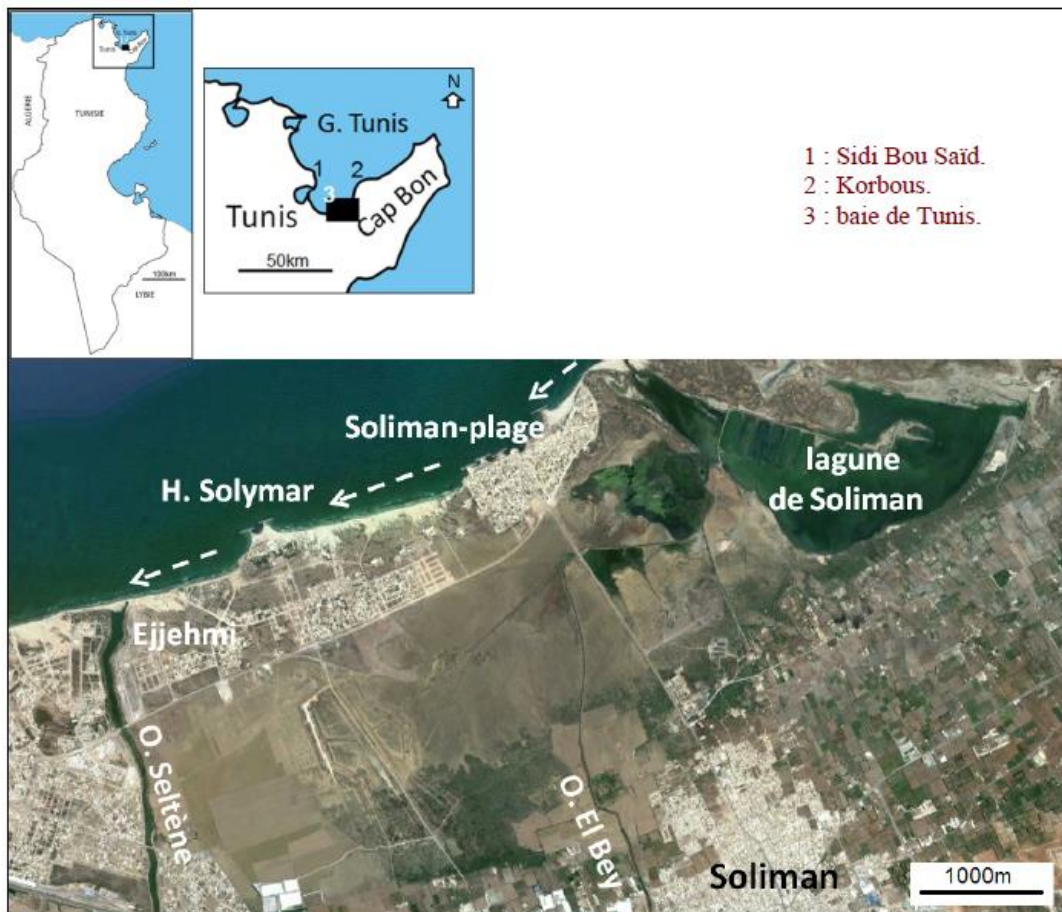


Figure 8. Soliman beach geographical location. Source: Marzougui et Oueslati 2017

Comparison with Marzougui (2017).

We have matched the two closest transects from our Tunisia analysis (Figure 9a) to each of the transects (A1 to E3) in the Marzougui (2017) study (Figure 9b) to compare change rates. These, as shown in Figure 9. Enabling a comparison of the erosion/accretion rates across the images transects. Table 3 provides the rates from 1948 to 2016 (Marzougui 2017) analysis alongside the recent values extracted for the same location.

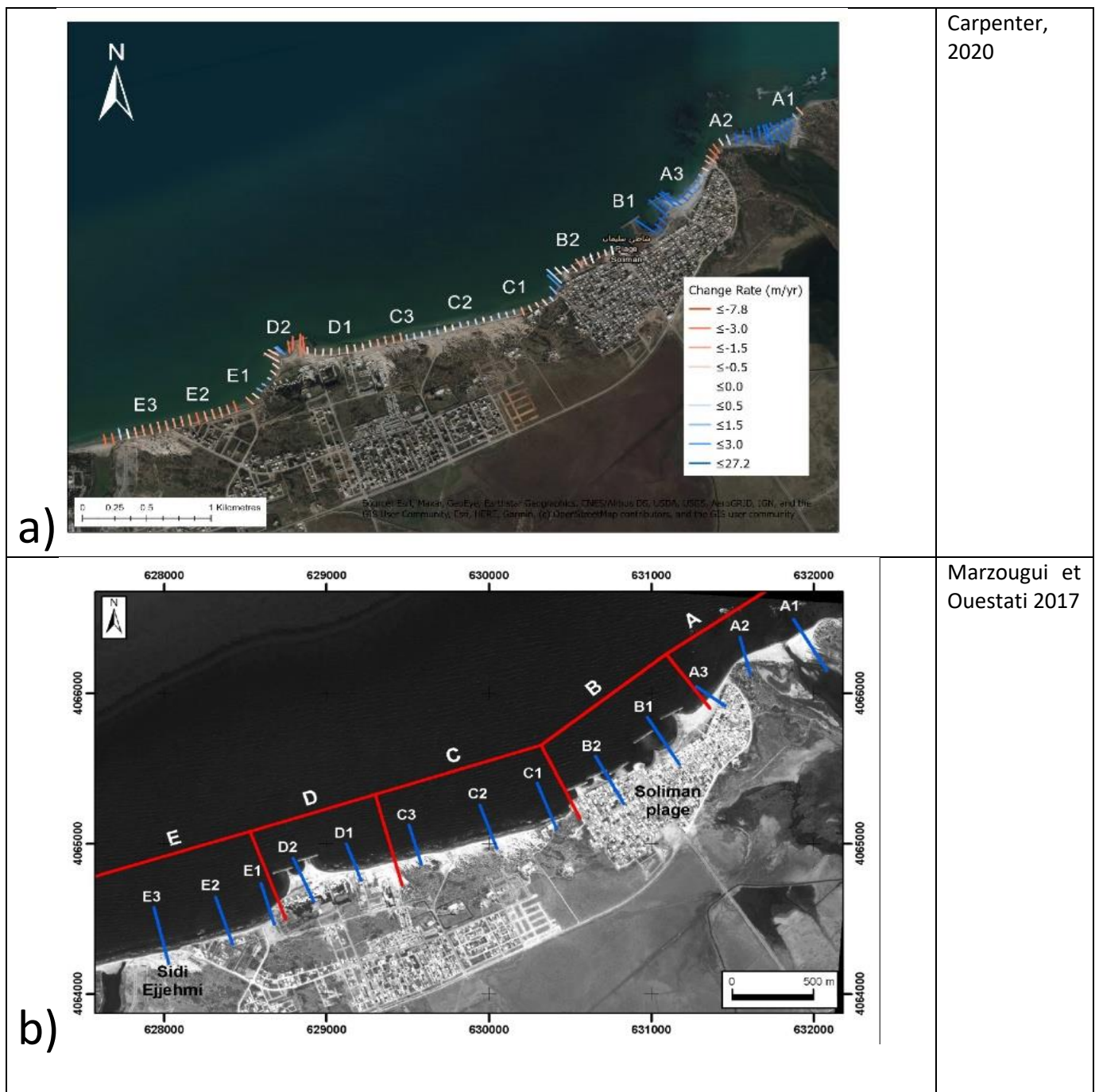


Figure 9. Soliman beach cross sectors of analysis

The images in Figure 9 provide a clear view of the replacement of breakwater in transect B2 and D2 and the surrounding erosion (E1, C1) and accretion rates (B1, A2, D1). All sections clearly show erosion along the entire coast from 1948 to 1996 (Table 3). The first set of engineering work for coastal infrastructure was implemented in 1990, indeed erosion rates were improved upstream of the structure as currents in the gulf of Tunis run westwards (sections A3, B1 in the period 1996 - 2016). Simultaneously, currents running westward would not deposit any sediments downstream of the structure; hence, erosion rates in section D and E worsen.

Table 3. Erosion rates across the Soliman beach cross sectors

Sector	Change Rate (m/yr)				
	Marzougui et al., 2017				Carpenter et al., 2020
	1948 - 1962	1962 - 1974	1974 - 1996	1996-2016	2000-2020
<b>A1</b>				<b>4.59</b>	<b>2.96</b>
<b>A2</b>			-0.82	<b>1.79</b>	<b>0.20</b>
<b>A3</b>	-2.4	-1	-2	<b>2.06</b>	<b>-0.42</b>
<b>B1</b>	-0.07	-2.25	-2.5		<b>0.99</b>
<b>B2</b>	0.28	-1.7	-1.8		<b>-1.18</b>
<b>C1</b>	-0.07	-0.5	-5	<b>-2.48</b>	<b>0.96</b>
<b>C2</b>	0.71	-1.8	-4	<b>-1.96</b>	<b>-0.96</b>
<b>C3</b>	0.21	-1	-2.4	<b>-1.75</b>	<b>-2.24</b>
<b>D1</b>	0.07	-1.6	-0.5	<b>-1.15</b>	<b>-1.68</b>
<b>D2</b>					<b>-3.74</b>
<b>E1</b>	0.21	-1.5	-3	<b>-3.70</b>	<b>-2.51</b>
<b>E2</b>	0.79	-1.5	-0.36	<b>-3.81</b>	<b>-3.32</b>
<b>E3</b>	1.3	-2.2	-2.2	<b>-4.63</b>	<b>-3.14</b>

The coastal breakwaters were replaced by coastal groynes in late 2018 (Figure 10). These findings show that sectors A3 and B1 experience higher accretion rates and beach replenishment. This demonstrates the immediate effect of currents transporting sediment, which is trapped upstream of the perpendicular structural groyne. Likewise, the structural groyne has had a positive effect downstream, the coastline continues to erode, but at a slower rate. Sectors C1 and E1 experience a replenishment of over 1.5 meters between 1996 and 2020.



Figure 10. Breakwater protection system (left), Groyne structures (right)

Development of groynes (2017-2018) / change from breakwater

The effect of the recent groyne system on sediment transport and distribution can be observed in Figures 11 and 12. These two figures show the same location divided into two sections, allowing closer examination. Graphs display the distance of the coastline each year from the baseline (2000). The graphs clearly show the accretion which occurs in 2018, particularly at transect 2 in Figure 11. The base map in these figures is from May 2017. This demonstrates the impact of the new developments and regeneration of the beach to the original baseline.

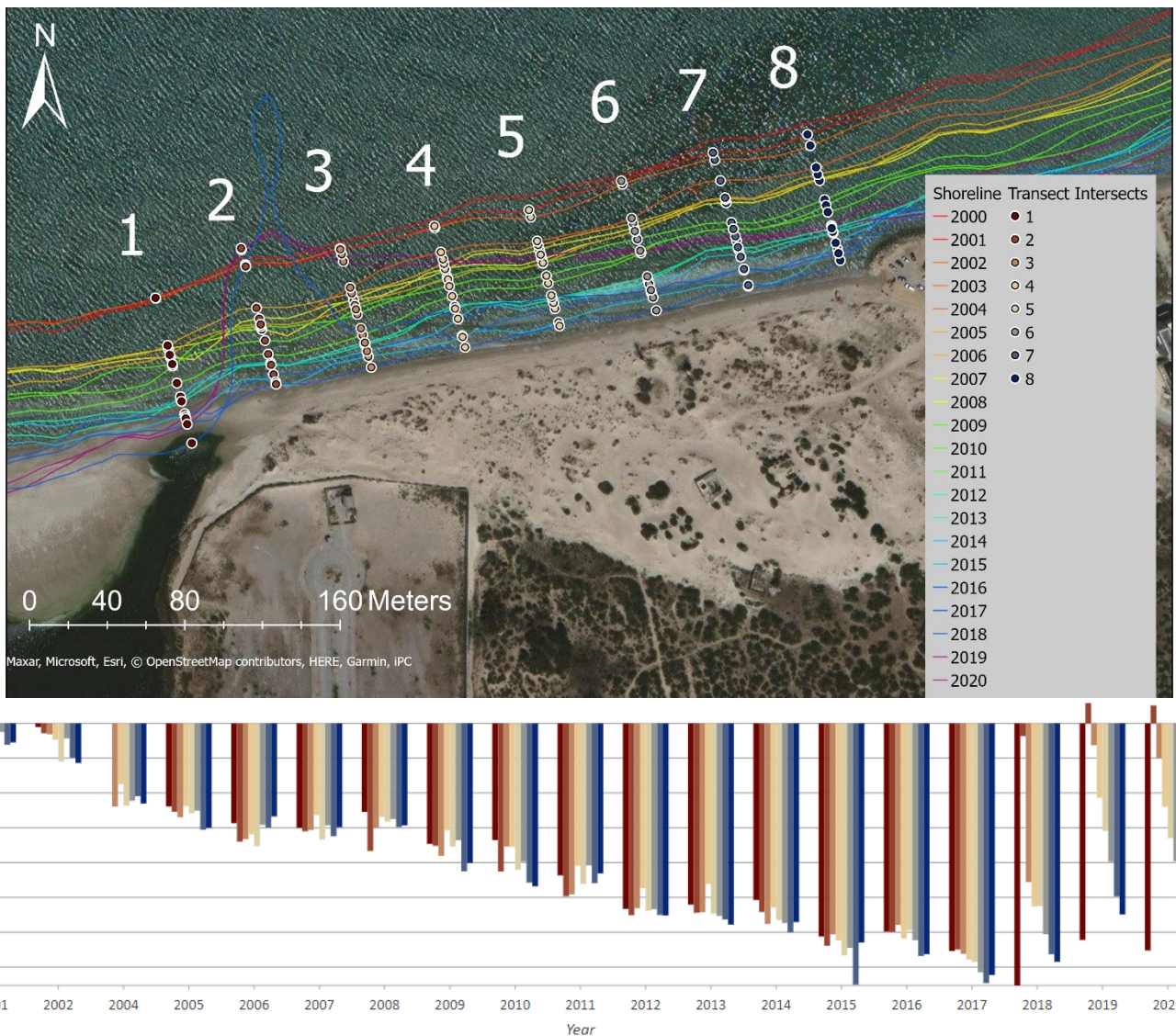


Figure 11. Coastline changes 2000-2020 from a groyne development with bar graph corresponding to the distance from the 2000 baseline to 2020.

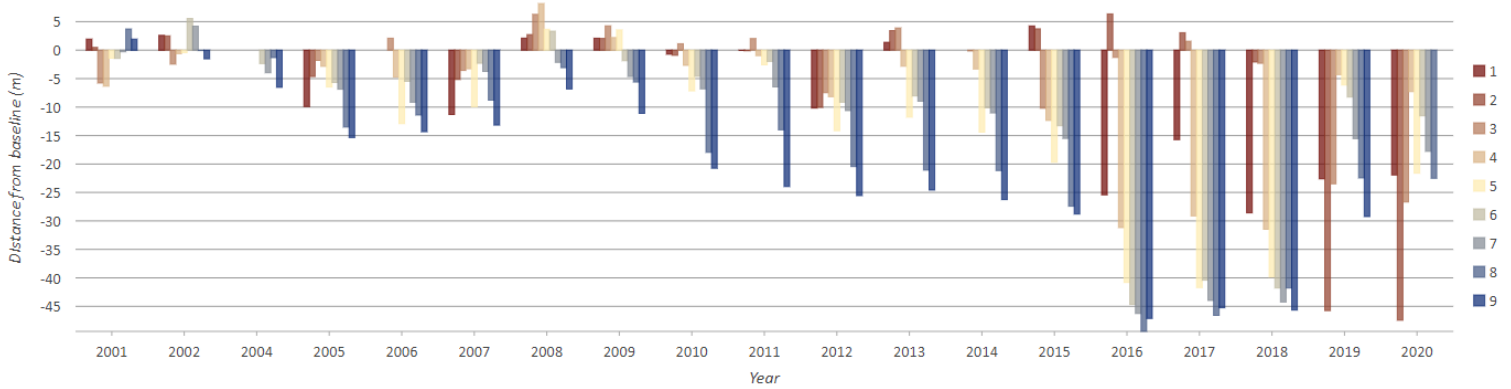
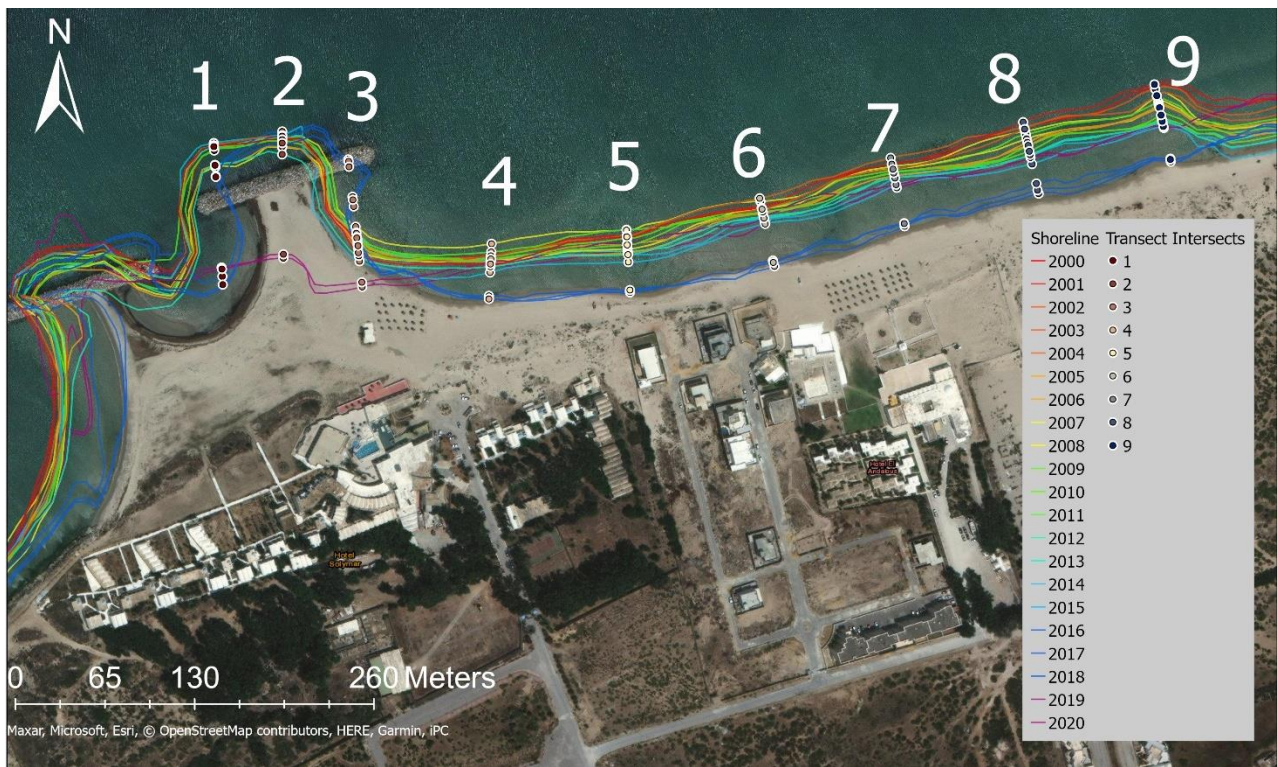


Figure 12 Coastal line changes 2000-2020 from the change from breakwater to groyne with bar graph corresponding to the distance from the 2000 baseline to 2020.

### Reflection points

- In situ data can validate the effects of coastal infrastructure on erosion and accretion zones. It can also support preliminary feasibility work for coastal zone infrastructure and nature-based solutions for adaptation. Adaptation options, notably those including hard infrastructure need to be pre-evaluated for feasibility and environmental impact assessments should be carried out
- Nature-based solutions for coastal adaptation must be considered and potentially combined with infrastructure protection as needed
- Patterns in the current dynamics, sediment transportation patterns, and sediments quantities need to be assessed for proper adaptation and management plans.

#### 4. Recommendations

As highlighted in the introduction, this study is unvalidated i.e. no in situ data has been obtained to validate the analysis. Validation is therefore recommended, ideally by comparison with existing in situ beach survey records over the time periods considered in the report (if available).

Future investigations could dig deeper into the temporal variability in the shoreline change rates. One option is to split the analysis by satellite time periods to reduce the positional uncertainty that occurs when calculating shoreline change using a combination of different satellites. Though this will increase processing time, maintaining the same spatial resolution would ensure that pixels align. Analysing more recent shoreline change (after the launch of Sentinel 2 in July 2015) is ideal at a constant 10m spatial resolution.

An interactive visual representation of this data could also be developed to facilitate the layering of visual information helping to explore the various drivers of change. As illustrated by the example at the Solymar beach area, human intervention or sudden natural events can result in misleading aggregated change rates. Localised views which include Intentional human interactions with the coast should be accounted for when understanding evolution rates as a linear regression over the entire period will not capture these sudden changes.

Manipulating the data to illustrate hotspots using algorithms such as Getis-Ord  $G_i^*$  (2010) will provide more easily interpretable assessments of specific locations which could be selected based on the highest rates of change, or for locations with high value or critical infrastructure. Local infrastructure data could be added to quantify the value of infrastructure that may be at risk when assuming scenarios under 'no active intervention'. This information would form a central component both as a decision support tool for local governments and a measure of performance of coastal defences.

A large proportion of North Africa has a sandy coastline, therefore the *Coastsat* algorithm is an effective method to provide information on shoreline change over time. However, a full validation study including both sandy and non-sandy coastlines, including beach profiles for the former is advised. There is also a need to refine the workflow used in this study by adding an automated filtering and baseline extraction process, which would increase the confidence level. Currently transects and shorelines are manually removed through a slow procedure where erroneous shorelines can be missed. Correcting this part of the workflow would also prevent gaps where a baseline could not be extracted.



## 5. References

- Amrouni, O., Hzami, A. and Heggy, E., 2019. Photogrammetric assessment of shoreline retreat in North Africa: Anthropogenic and natural drivers. *ISPRS Journal of Photogrammetry and Remote Sensing*, 157, pp.73-92.
- Athanasiou, P., Van Dongeren, A., Giardino, A., Voutsoukas, M., Gaytan-Aguilar, S. and Ranasinghe, R., 2019. Global distribution of nearshore slopes with implications for coastal retreat. *Earth system science data*, 11(4) - <https://data.4tu.nl/repository/uuid:a8297dcd-c34e-4e6d-bf66-9fb8913d983d>
- Ayache, F., Thompson, J.R., Flower, R.J., Boujarra, A., Rouatbi, F. and Makina, H., 2009. Environmental characteristics, landscape history and pressures on three coastal lagoons in the southern Mediterranean region: Merja Zerga (Morocco), Ghar El Melh (Tunisia) and Lake Manzala (Egypt). *Hydrobiologia*, 622(1), pp.15-43.
- Benkhatab, F.Z., Hakkou, M., Bagdanavičiūtė, I., El Mrini, A., Zagaoui, H., Rhinane, H. and Maanan, M., 2020. Spatial–temporal analysis of the shoreline change rate using automatic computation and geospatial tools along the Tetouan coast in Morocco. *Natural Hazards*, pp.1-18.
- Berraho, A., Abdelouahab, H., Larissi, J., Baibai, T., Charib, S., Idrissi, M., Belbchir, Y., Ettahiri, O. and Hilmi, K., 2019. Biodiversity and spatio-temporal variability of copepods community in Dakhla Bay (southern Moroccan coast). *Regional Studies in Marine Science*, 28, p.100437.
- Chander, G., Markham, B.L. and Helder, D.L., 2009. Summary of current radiometric calibration coefficients for Landsat MSS, TM, ETM+, and EO-1 ALI sensors. *Remote sensing of environment*, 113(5), pp.893-903.
- Chekirbane, A., Tsujimura, M., Kawachi, A., Isoda, H., Tarhouni, J. and Benalaya, A., 2013. Hydrogeochemistry and groundwater salinization in an ephemeral coastal flood plain: Cap Bon, Tunisia. *Hydrological Sciences Journal*, 58(5), pp.1097-1110.
- Cipolletti, M.P., Delrieux, C.A., Perillo, G.M. and Piccolo, M.C., 2012. Superresolution border segmentation and measurement in remote sensing images. *Computers & geosciences*, 40, pp.87-96.
- Civco, D.L., 1993. Artificial neural networks for land-cover classification and mapping. *International journal of geographical information science*, 7(2), pp.173-186.
- Coastalcare.org. 2020. *The Sand Thieves Of Larache, Northern Morocco | Coastal Care*. [online] Available at: <<https://coastalcare.org/2015/10/the-sand-thieves-of-larache-northern-morocco/>> [Accessed 18 September 2020].
- Data.humdata.org. 2020. *Humanitarian Data Exchange*. [online] Available at: <<https://data.humdata.org/dataset>> [Accessed 1 June 2020].
- Data.un.org. 2020. *United Nations Population Division*. [online] Available at: <<http://data.un.org/Data.aspx?q=morocco&d=PopDiv&f=variableID%3a12%3bcrID%3a504>> [Accessed 12 August 2020].

Demirkesen, A.C., Evrendilek, F. and Berberoglu, S., 2008. Quantifying coastal inundation vulnerability of Turkey to sea-level rise. *Environmental Monitoring and Assessment*, 138(1-3), pp.101-106.

Eliason, M., 2020. *UN Report: Sand Mafias Are Destroying Moroccan Beaches*. [online] Morocco World News. Available at: <<https://www.moroccoworldnews.com/2019/05/272951/un-sand-mafias-moroccan-beaches/>> [Accessed 11 August 2020].

Esteves, L.S. and Finkl, C.W., 1998. The problem of critically eroded areas (CEA): An evaluation of Florida beaches. *Journal of Coastal Research*, pp.11-18.

Gao, F.; Masek, J.G.; Wolfe, R.E. Automated registration and orthorectification package for Landsat and Landsat-like data processing. *J. Appl. Remote Sens.* 2009, 3, 033515

Getis, A. and Ord, J.K., 2010. The analysis of spatial association by use of distance statistics. In *Perspectives on spatial data analysis* (pp. 127-145). Springer, Berlin, Heidelberg.

Ghosh, M.K., Kumar, L. and Roy, C., 2015. Monitoring the coastline change of Hatiya Island in Bangladesh using remote sensing techniques. *ISPRS Journal of Photogrammetry and Remote Sensing*, 101, pp.137-144.

Gloss-sealevel.org. 2021. *GLOSS | The Global Sea Level Observing System*. [online] Available at: <<https://www.gloss-sealevel.org/>> [Accessed 8 August 2020].

Hanen Saidi, Radhia Souissi, Fouad Zargouni, 2012. Environmental impact of detached breakwaters on the Mediterranean coastline of Soliman (North-east of Tunisia).

Hayes, M.O. and FitzGerald, D.M., 2013. Origin, evolution, and classification of tidal inlets. *Journal of Coastal Research*, (69), pp.14-33.

Himmelstoss, E.A., Henderson, R.E., Kratzmann, M.G., and Farris, A.S., 2018, Digital Shoreline Analysis System (DSAS) version 5.0 user guide: U.S. Geological Survey Open-File Report 2018–1179, 110 p., <https://doi.org/10.3133/ofr20181179>.

INS (Tunisian National Institute of Statistic), 2014. Statistic of the Population Urban growth in the Nabeul Governorate. <http://www.nabeul.gov.tn/fr/donnees-generales/donnees-demographiques/>.

IPCC Climate Change (2014) Synthesis report. In: Contribution of Working Groups I, II and III to the Fifth Assessment Report of the Intergovernmental Panel on Climate Change. Geneva, Switzerland, pp 151

Kalman, R.E., 1960. A new approach to linear filtering and prediction problems.

Kasmi, S., Snoussi, M., Khalfaoui, O., Aitali, R. and Flayou, L., 2020. Increasing pressures, eroding beaches and climate change in Morocco. *Journal of African Earth Sciences*, 164, p.103796.

Kouzana, L. and Benassi, R., 2010. Geophysical and hydrochemical study of the seawater intrusion in Mediterranean semi arid zones. Case of the Korba coastal aquifer (Cap-Bon, Tunisia). *Journal of African Earth Sciences*, 58(2), pp.242-254.

Landsat.gsfc.nasa.gov. 2020. *The Worldwide Reference System*. [online] Available at: <<https://landsat.gsfc.nasa.gov/the-worldwide-reference-system/>> [Accessed 7 August 2020].

Long, J.W., and Plant, N.G., 2012, Extended Kalman Filter framework for forecasting shoreline evolution: *Geophysical Research Letters*, v. 39, no. 13, p. 1–6.

Luijendijk, A., Hagenaars, G., Ranasinghe, R., Baart, F., Donchyts, G. and Aarninkhof, S., 2018. The state of the world's beaches. *Scientific reports*, 8(1), pp.1-11.

Marzougui, W. and Oueslati, A., 2017. The beaches of the coast of Ejehmi-Soliman (Gulf of Tunis, Tunisia): example of acceleration of marine erosion in an artificially split sediment cell. *Physio-Geo. Physical geography and environment*, (Volume 11), pp. 21-41.

Nguyen, M.D., Baez-Villanueva, O.M., Bui, D.D., Nguyen, P.T. and Ribbe, L., 2020. Harmonization of Landsat and Sentinel 2 for Crop Monitoring in Drought Prone Areas: Case Studies of Ninh Thuan (Vietnam) and Bekaa (Lebanon). *Remote Sensing*, 12(2), p.281.20].

Ordnance Survey, 2020. *UK GEOS Coastal Erosion And Accretion Project*. [online] p.17. Available at: <<https://spaceforsmartergovernment.uk/workspace/assets/files/coastal-erosion-and-accretion-5afd7a8fbf023.pdf>> [Accessed 3 June 2020].

Otsu, N., 1979. A threshold selection method from gray-level histograms. *IEEE transactions on systems, man, and cybernetics*, 9(1), pp.62-66.

Pardo-Pascual, J.E., Sánchez-García, E., Almonacid-Caballer, J., Palomar-Vázquez, J.M., Priego De Los Santos, E., Fernández-Sarría, A. and Balaguer-Beser, Á., 2018. Assessing the accuracy of automatically extracted shorelines on microtidal beaches from Landsat 7, Landsat 8 and Sentinel-2 imagery. *Remote Sensing*, 10(2), p.326.

Pro.arcgis.com. 2020. *Central Feature—Arcgis Pro | Documentation*. [online] Available at: <<https://pro.arcgis.com/en/pro-app/tool-reference/spatial-statistics/central-feature.htm>> [Accessed 3 June 2020].

Saïdi, H., Souissi, R. and Zargouni, F., 2012. Environmental impact of detached breakwaters on the Mediterranean coastline of Soliman (North-East of Tunisia). *Rendiconti Lincei*, 23(4), pp.339-347.

Snoussi, M., Ouchani, T. and Niazi, S., 2008. Vulnerability assessment of the impact of sea-level rise and flooding on the Moroccan coast: the case of the Mediterranean eastern zone. *Estuarine, Coastal and Shelf Science*, 77(2), pp.206-213.

Snoussi, M., Ouchani, T., Khouakhi, A. and Niang-Diop, I., 2009. Impacts of sea-level rise on the Moroccan coastal zone: quantifying coastal erosion and flooding in the Tangier Bay. *Geomorphology*, 107(1-2), pp.32-40.

Snoussi, M., Ouchani, T., Khouakhi, A. and Niang-Diop, I., 2009. Impacts of sea-level rise on the Moroccan coastal zone: quantifying coastal erosion and flooding in the Tangier Bay. *Geomorphology*, 107(1-2), pp.32-40.

Sytnik, O., Del Río, L., Greggio, N. and Bonetti, J., 2018. Historical shoreline trend analysis and drivers of coastal change along the Ravenna coast, NE Adriatic. *Environmental Earth Sciences*, 77(23), p.779.

Taaouati, M., Anfuso, G. and Nachite, D., 2015. Morphological characterization and evolution of Tahadart littoral spit, Atlantic coast of Morocco. In *Sand and Gravel Spits* (pp. 289-306). Springer, Cham.

Tu, T.M., Su, S.C., Shyu, H.C. and Huang, P.S., 2001. A new look at IHS-like image fusion methods. *Information fusion*, 2(3), pp.177-186.

Unsalb.org. 2021. Home | Second Administrative Level Boundaries. [online] Available at: <<https://www.unsalb.org/#:~:text=The%20Second%20Administrative%20Level%20Boundaries,the%20National%20Geospatial%20Information%20Authorities.>> [Accessed 8 January 2021].

Vos, K., 2019. Training data for: *Coastsat* image classification. Zenodo Digital Repository <https://doi.org/10.5281/zenodo.3334147>

Vos, K., Harley, M.D., Splinter, K.D., Simmons, J.A. and Turner, I.L., 2019b. Sub-annual to multi-decadal shoreline variability from publicly available satellite imagery. *Coastal Engineering*, 150, pp.160-174.

Vos, K., Splinter, K.D., Harley, M.D., Simmons, J.A. and Turner, I.L., 2019a. *Coastsat*: A Google Earth Engine-enabled Python toolkit to extract shorelines from publicly available satellite imagery. *Environmental Modelling & Software*, 122, p.104528.

Xu, H., 2006. Modification of normalised difference water index (NDWI) to enhance open water features in remotely sensed imagery. *International journal of remote sensing*, 27(14), pp.3025-3033.

Zghibi, A., Zouhri, L. and Tarhouni, J., 2011. Groundwater modelling and marine intrusion in the semi-arid systems (Cap-Bon, Tunisia). *Hydrological processes*, 25(11), pp.1822-1836.

## Annex A: Detailed Description of Methodology

The methodology adopted for the analysis draws on two scientific tools. Firstly, *Coastsat*, an open-source software toolkit, delineates shorelines at any sandy coastline worldwide from over 30 years of publicly available satellite imagery (<https://github.com/kvos/Coastsat>). The toolkit applies a similar method to Luijendijk et al. (2018), using yearly composites of Landsat and Sentinel 2 data to explore change at a higher level of spatial detail of 50m intervals between transects. The *Coastsat* tool was chosen as it is a quick and easy to use code, which enables the exploration and monitoring of coastlines. Validation of the tool produces a cross-shore accuracy of satellite-derived shorelines relative to field surveys, from 7.3m at a micro-tidal site with a steep-sloping beach face, and up to 12.7m at a meso-tidal site with a gently sloping beach slope (Vos et al., 2019b). This was deemed an acceptable level of accuracy to explore shoreline change across two decades and forecast for a further two. The modification of the algorithm to include yearly median composites was expected to increase this accuracy, though it is unvalidated in this report.

The use of median composites within the analysis targets difficulties associated with; cloud cover in images, combats tidal differences by averaging over the year, and increase the data available for analysis despite the scan line error in Landsat 7. With the efficiency in downloading a subset of data using Google Earth Engine (GEE), small regions can be analysed using a laptop with relatively basic processing power in a short time.

The *Coastsat* repository contains code to perform coastal change analysis, by drawing, importing or providing coordinates of transects. Here, we exploit the breadth of statistical outputs and handy visualization and forecasting tools in the second scientific tool; the Digital Shoreline Analysis System (DSAS). This is a freely available ArcMap plug-in tool for calculating shoreline change statistics from multiple historical shoreline positions; created as a central component of a USGS project, 'U.S. Geological Survey's Coastal Change Hazards'. This tool was chosen as it provides a quick and easily repeatable method for calculating regression rates over large volumes of data.

This report includes a summary of the methods in both tools in the context of North Africa, whilst noting the modifications made to the *Coastsat* algorithm. The complete original approach and user guide can be accessed here:

- *Coastsat* - *Coastsat*: A Google Earth Engine-enabled Python toolkit to extract shorelines from publicly available satellite imagery (Vos et al., 2019a). Information on the tool's applications, including accuracy, are discussed in *Sub-annual to multi-decadal shoreline variability from publicly available satellite imagery* (Vos et al., 2019b).
- *DSAS* – Digital Shoreline Analysis System (DSAS) version 5.0 user guide (Himmelstoss et al., 2018).

A summary of the workflow using both tools is summarised by Figure i.

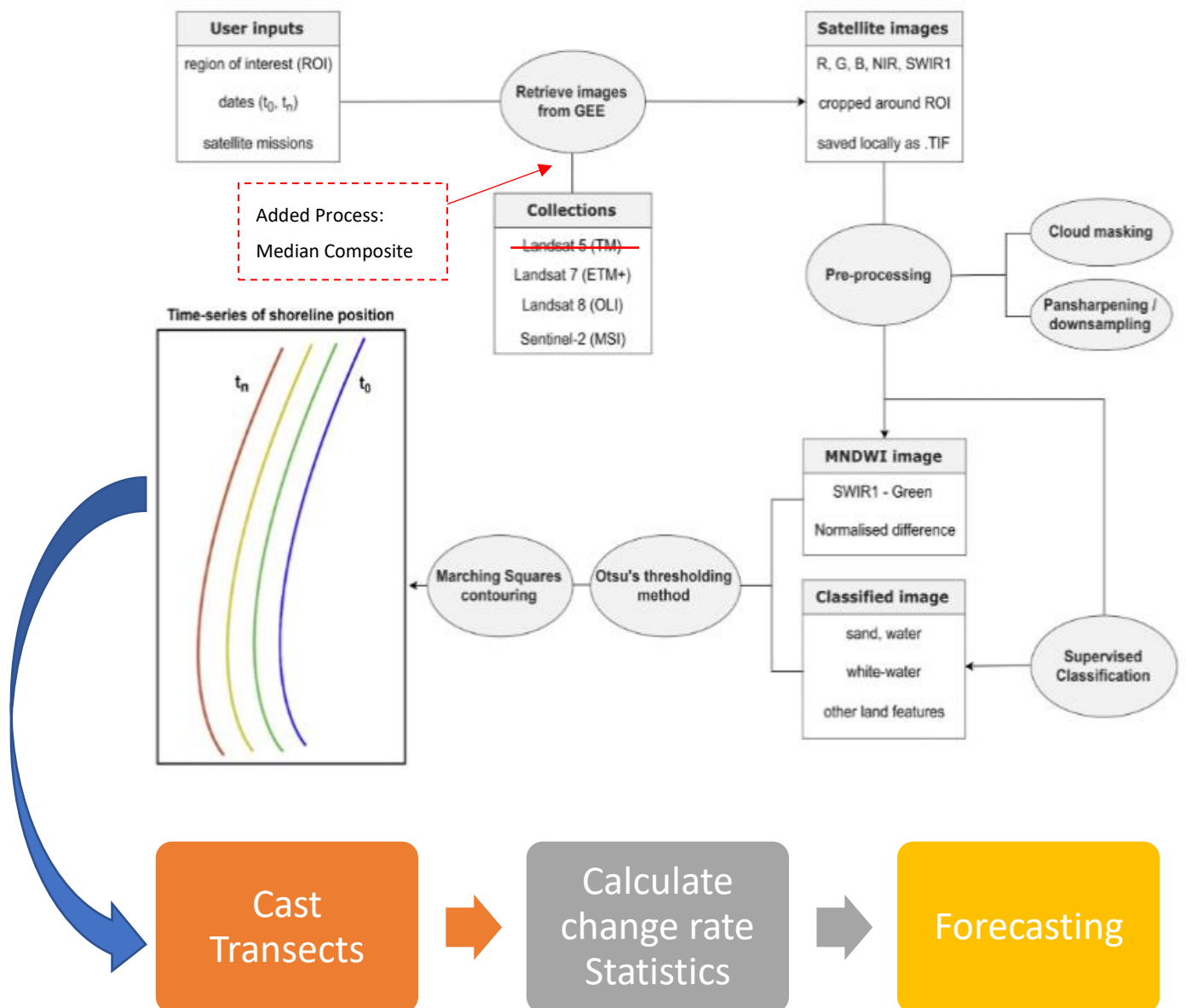


Figure i. Flow diagram outlining the steps within Coastsat. Edited. Original source: Vos et al., 2019a

**IMPORTANT:** The outputs from this report are not validated by ground truth data (e.g. GPS beach transects), therefore figures and statistics should be used as a guide and may not be accurate at a local scale. Forecasts are based on simple linear functions which rely on historical data not new developments. It is recommended that forecast lines should be presented with the uncertainty band. Exploring the shorelines at each year may explain irregularities in the forecast or change rates. This is one of the key areas of future work to determine accuracy statistics for shorelines using local tidal and current data to provide a higher-level quality data to local decision-makers.

### *Delineating the Shoreline: Coastsat*

#### *Retrieval of the images from the Google Earth Engine archive*

Data providers usually have multiple tiers of satellite images available. TOA (Top-of-Atmosphere) reflectance images provide a standardised comparison between images (Chander et al., 2009). This is the same for Sentinel-2, where quality-controlled TOA reflectance images that are suitable for time-series analysis (ESA, 2015).

The *Coastsat* algorithm is limited to process 100km<sup>2</sup> per image due to file download restraints from GEE. Therefore, to process the shorelines over an entire country, the shoreline was split into smaller areas along the coast. Four coordinates were used to describe these regions. These were derived by downloading the administrative boundaries from the Humanitarian Data Exchange (Humanitarian Data Exchange, 2020); the source and timestamp of each country's boundary data is dependent on its location. The boundary line along the shore was assumed to be accurate within 1km, as a series of rectangular boxes (approximately 2\*11km) was then created along these lines. A manual check was completed to ensure that all the shoreline was incorporated inside each box. The maximum x,y coordinates of these boxes, further referred to as regions of interest (ROIs) were exported as a list, which were used to define the areas of satellite imagery to download.

Annual median composites for each year between 2000 and 2020 were processed on GEE. Images from the following dates and corresponding satellites were then downloaded for further processing:

- Landsat 7 (ETM) – 2000-2013
- Landsat 8 (OLI) – 2014, 2015
- Sentinel-2 (MSI) – 2016 - 2020

Before downloading, Landsat images require co-registration. Misalignment between Landsat and Sentinel images can exceed 38m due to the difference in georeferencing framework. Therefore, the functions 'displacement' and 'displace' are used to perform a 'rubber-sheet' deformation over each region of interest along the coast. Two single, cloud-minimal (below 20%) Landsat and Sentinel images are chosen from a two-month period in 2016, and used to identify the XY displacement vectors through computer generates ground control points. The XY displacement output is then applied to the rest of the Landsat images in that region. This method assumes displacement between Sentinel and Landsat images in 2016 are constant across all Landsat images. Further details on the methods behind the displace and displacement functions in GEE are not documented clearly, but according to Nguyen et al. 2020, further details are described in Gao et al. 2009 for a similar tool called AROP which is an open-source package.

Once downloaded, the quality assessment layer for each satellite was used to determine a percentage cloud cover. The shoreline detection algorithm creates as many valid shorelines as possible after considering a cloud threshold of 95%. Despite the use of the median filter, clouds may persist in particularly prevalent areas or those with limited satellite images available. Images between 2003-2014 included missing data due to Landsat 7's scan line error; some of which was filled with the median function as the scan error moves throughout the year. This data was processed in August 2020, therefore the shoreline delineated at 2020 only represents the first half of the year.

### Pre-processing: Pan sharpening and down-sampling

The higher resolution panchromatic band from Landsat 7 and 8 is used to increase the resolution of the bands from 30m to 15m by applying a data fusion method based on principal component analysis (Tu et al., 2001). Multispectral bands are down-sampled to 15m (by bilinear interpolation) and decomposed in principal components, then the first principal component is replaced by the panchromatic band (after matching the histograms) and retransformed back into the original multispectral space. For Sentinel-2 images, the 20 m SWIR1 band is down-sampled to 10m by bilinear interpolation, so that all the bands are at 10m resolution (Vos et al., 2019a).

### Shoreline detection

The shoreline is detected by performing a classification and segmentation. A Neural Network classifier (Civco, 1993), is used to label each pixel of the image with one of four classes: 'sand', 'water', 'white-water', 'other land features' (e.g., vegetation, buildings, rocky headlands). The individual class of white-water allows this to be removed so that areas can be mapped effectively, irrelevant to the presence of white-water or urban areas. 20 explanatory variables are used as inputs for the classifier, these include the pixel intensity in 5 multispectral bands (i.e., R, G, B, NIR, SWIR1), 5 commonly used spectral indices and the variance (calculated using a 3x3 moving window) of each multispectral band and spectral index. A set of 500 training pixels were manually trained from 50 satellite images (Vos 2019) and are used to classify the newly downloaded images. Sub-pixel border segmentation is used to extract the boundary between sand and water. Modified Normalized Difference Water Index (MNDWI) (Xu, 2006) is applied to each of the classified images and is calculated as follows:

$$\text{MNDWI} = (\text{SWIR1} - \text{G}) / (\text{SWIR1} + \text{G})$$

Otsu's thresholding algorithm (Otsu, 1979) is used to discriminate the MNDWI value that maximises the inter-class variance between 'sand' and 'water'. Figure ii illustrates a subsection at the sand/water boundary, which includes white-water and other land features. Removing the latter classes results in an Otsu's threshold of  $\sim -0.1$ ; this is the probability density function (PDF). Finally, an iso-valued contour is computed on the MNDWI image for a level equal to the 'sand' / 'water' threshold. This operation is done at sub-pixel resolution by applying the Marching Squares algorithm (Cipolletti et al., 2012) and delineates the mean high-water mark. A similar methodology to Vos et al. (2019a) is applied; with the use of a water difference index, a classification and a contouring method to distinguish a shoreline boundary.

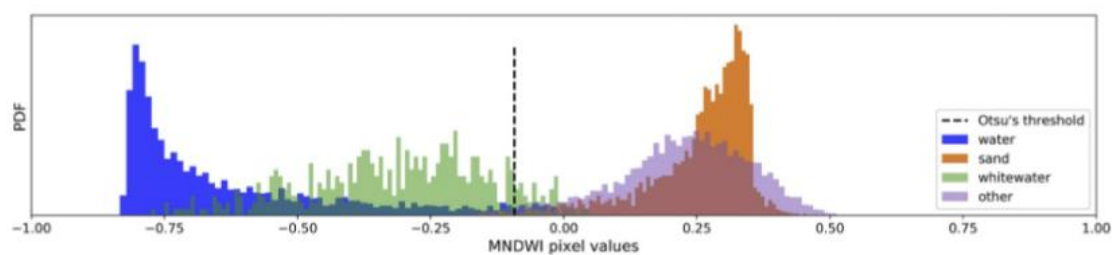
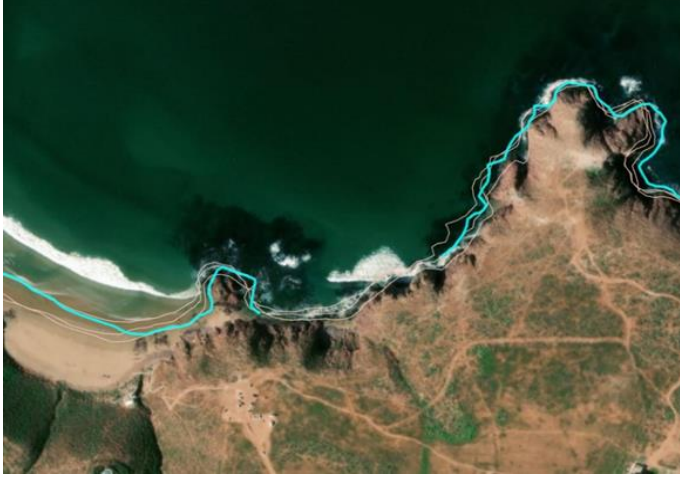


Figure ii. MNDWI pixel values from a small region of interest at the sand-water boundary; Source: Vos et al, 2019a



Table 1. Removing false shorelines due to clouds.

Basemap source: ArcGIS Basemap (2013) - Esri, DigitalGlobe, GeoEye, i-cubed, USDA FSA, USGS, AEX, Getmapping, Aerogrid, IGN, IGP, swisstopo, and the GIS User Community)

Shoreline Error	Fix
<p data-bbox="108 329 743 533">Clouds may persist within the buffer region along the coast. The boundaries between the cloud and water are reflected in the MNDWI value, which is similar to the characteristics of sand and land. This leaves artefacts within the polyline.</p> 	<p data-bbox="770 329 1458 405">Cloud artefacts are cut out and the shoreline is split into two lines.</p> 

### *Cleaning and filtering*

Having just restricted the satellite images by a cloud cover threshold, the algorithm delineates false shorelines on surrounding the edges of clouds or the boundary between shadows (e.g. on mountainous regions). This is because they share similar spectral characteristics as the sand/water boundary. These are removed by creating a buffer around the administrative boundary shoreline of 1km. All shorelines which are not fully contained within this buffer are removed from further analysis. A further manual cleaning process is needed to remove lines within this buffer (Table 1). Each shoreline ROI is then merged to create a single dataset for the entire country. This dataset becomes the input into the DSAS workflow, which is briefly described in the next section.

### *Shoreline Change Statistics (DSAS)*

Digital Shoreline Analysis System is a freely available software application that works within the Esri Geographic Information System (ArcGIS) software. DSAS computes rate-of-change statistics for a time series of shoreline vector data. Here, we briefly describe the methods involved in the process, for more information please refer to the full guide (<https://pubs.usgs.gov/of/2018/1179/ofr20181179.pdf>). The following process contains four main stages:

1. Creating a baseline
2. Casting Transects
3. Calculating Statistics
4. Forecasting

### *Creating a baseline*

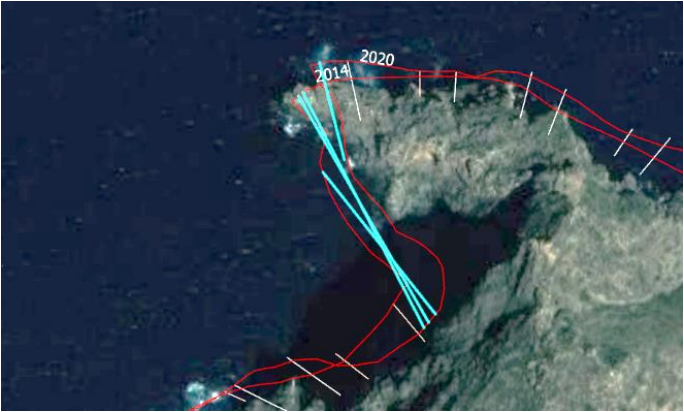
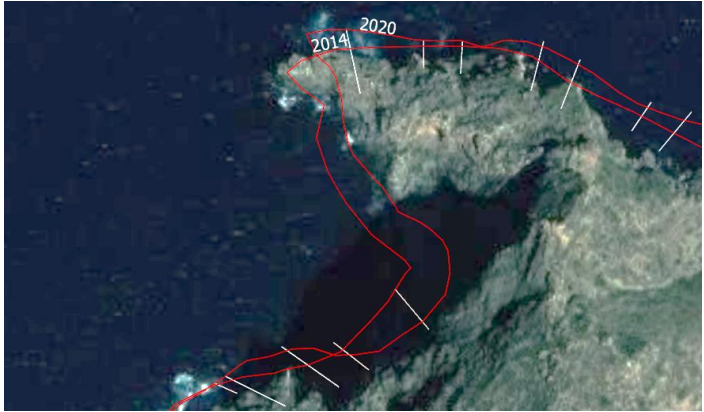


The baseline is created by selecting the shoreline in the year 2000 for each region of interest along the shoreline. This region of interest is the same area used to download each satellite image. In some areas of the shoreline this baseline was broken due to satellite data gaps, cloud presence or failed delineation of the shore. In these large gaps, the next earliest shoreline was substituted up to the year 2004, with the exception of the Island of Kerkennah, where satellite imagery was only available for Sentinel 2 therefore a baseline from 2015 was selected. Unfortunately, due to time restraints, small gaps in some areas remain. It was deemed that this baseline was more suitable to map shoreline change over other sources, such as the administrative line, which may be outdated or inaccurate.

### *Casting and editing transects*

The transects are cast from this baseline and clipped to the extent of the surrounding shorelines. The maximum search distance from the baseline in this casting process was set to 140m and the spacing between transects to 50m. A smoothing distance was set to 500; this impacts the change rate as large smoothing values result in a longer reference line and produce more uniform transect orientations (Himmelstoss et al., 2018). The optimal smoothing distance depends on how sinuous the coastline is, which was challenging to achieve at a country-scale. Nevertheless, a trial-and-error method was used on the Tunisia dataset to visualise the impact and make a judgement that was used when creating the transects for Morocco. Once created, a final visual check was completed to remove transects that did not follow the orientation of the shoreline or crossed multiple shorelines (i.e. those created on splits or piers). Transects were then classified as sandy/non-sandy by joining data within 500m from the global analysis of shoreline change by Luijendijk et al. (2018). The change rates from the global analysis were also carried forward so that comparisons could be made.

Table 2. Incorrectly orientated transects between shorelines.

Basemap source: ArcGIS Basemap (2013) - Esri, DigitalGlobe, GeoEye, i-cubed, USDA FSA, USGS, AEX, Getmapping, Aerogrid, IGN, IGP, swisstopo, and the GIS User Community)

Shoreline Error	Fix
<p data-bbox="92 481 805 593">A single smoothing value is used on the baseline, but this results in transects that may not reflect the orientation of the shoreline.</p> 	<p data-bbox="805 481 1543 548">These transects need to be removed to prevent false change rates.</p> 
<p data-bbox="92 1097 805 1254">Coastal inlets and dynamic environments result in many lines in close proximity (&lt;170m). Transects are created between some coastal formations, particularly in estuaries.</p> 	<p data-bbox="805 1153 1543 1198">Interlocking transects are removed.</p> 

### *Calculating change rate statistics*

To calculate change rates and forecast, linear regression is determined by fitting a least-squares line to the shoreline intersects with each transect. A change rate is only calculated when five shorelines intersect the transects. Linear regression uses all of the data available to place a line where the minimal sum of squared residuals occurs. This method leaves the change rate susceptible to outliers, which can be indicated by; the standard error of the estimate (LSE) and the standard error of the slope with a user-selected confidence interval (LCI95). Here, the confidence interval was set at 95%. A 'Completeness' statistics is determined by spatially joining the data to within 500m to transects created by Luijendijk et al. (2018) which was assumed to be a comprehensive dataset.

### *Beta Shoreline Forecasting*

DSAS forecasts the shoreline uses the linear regression rate to calculate the future position of the shoreline, this is limited to two periods; 10yrs and 20yrs. This uses a Kalman filter (Kalman, 1960) to combine observed shoreline positions with model-derived positions. This begins at the first time-step (2000) and predicts the shoreline position for each successive time step until another shoreline observation is encountered (Himmelstoss et al., 2018). At this point, the model uses a Kalman filter to minimize the error between the modelled and observed shorelines to improve the forecast, including updating the rate and uncertainties (Long and Plant, 2012). As noted in the user guide, this forecast should always be used with caution as it does not account for the complex processes driving shoreline change and assumes a linear regression is valid. As part of the forecast, and an uncertainty for each shoreline - set at the U.S Geological Survey suggestion of 10m – is used to create an uncertainty region at which the shoreline may lie within at 95% confidence. Total change area statistics were calculated by extracting the shoreline created in the latest year [2020] and developing overlapping polygons of accretion and erosion for the 10 and 20-year forecast. The sum of these areas per country/area is reported in the results.

### *Limitations*

Despite using a median and as a result of the data gap in Landsat 7, some images produce broken lines along the shore. Therefore, when extracting the baseline, some areas fail to have a baseline recording. Whilst there may be other shorelines available, a full baseline would require manual editing of vertices of lines across multiple years. Large gaps between 2000-recorded shorelines are manual filled, but time restraints prevent the maximum completeness of the baseline. Locations which have undergone massive change since 2000 can also be under-represented. For example, extending splits may reach beyond the 170m distance either side of the 2000 baseline. Shorelines at a local scale should be visualised to understand the evolution of change in these areas.

Multiple shorelines in a single year can also be mapped where the algorithm identifies multiple water/sand interfaces. This can protrude in the extraction of the baseline and current (2020) shoreline used to map erosion and accretion areas. This emphasises the shoreline change rate when interpreting the mean value across a region or nation.



Figure iii.3. Shorelines delineated in a non-sandy location, illustrating a significant difference between Sentinel 2 (blue) and Landsat 7 (Orange) and 8 (Green). Basemap source: ArcGIS Basemap (2013) - Esri, DigitalGlobe, GeoEye, i-cubed, USDA FSA, USGS, AEX, Getmapping, Aerogrid, IGN, IGP, swisstopo, and the GIS User Community)

Non-sandy coastlines are unvalidated and have been left out of the statistics in the results. The algorithm calculates a boundary from the sand-water interface which fails in non-sandy areas. Though some of these areas may show similar spectral characteristics of sand, there appears to be a significant, yet unknown, spatial difference between Sentinel 2 and the Landsat shorelines despite implementing a co-registration (Figure iii). Further investigation and algorithm refinement are required to include shoreline change rates in non-sandy areas.

Complex hydrodynamic areas of the shoreline such as river mouths or tidal inlets are often highly dynamic and makes calculating change in these areas difficult. For example, Dakhla Bay is a narrow inlet approximately 37km long and 12km wide located in Southern Morocco, which has a very low bathymetry less than 20m (Berraho et al., 2019). The hydrodynamics of the bay are governed by bidirectional tides and the wind which results in a shoreline which is hugely varied throughout the year. Figure 4 illustrates a subset of the bay where all the shorelines are mapped across the 20 years. The use of singular transects along a baseline is not a suitable method to determine a change as the shoreline varies in shape and direction every year. These areas require a more complex analysis to view changes over time. The use of a mean centre for individual years would help demonstrate overall shoreline movement in the area (also in Figure iv).

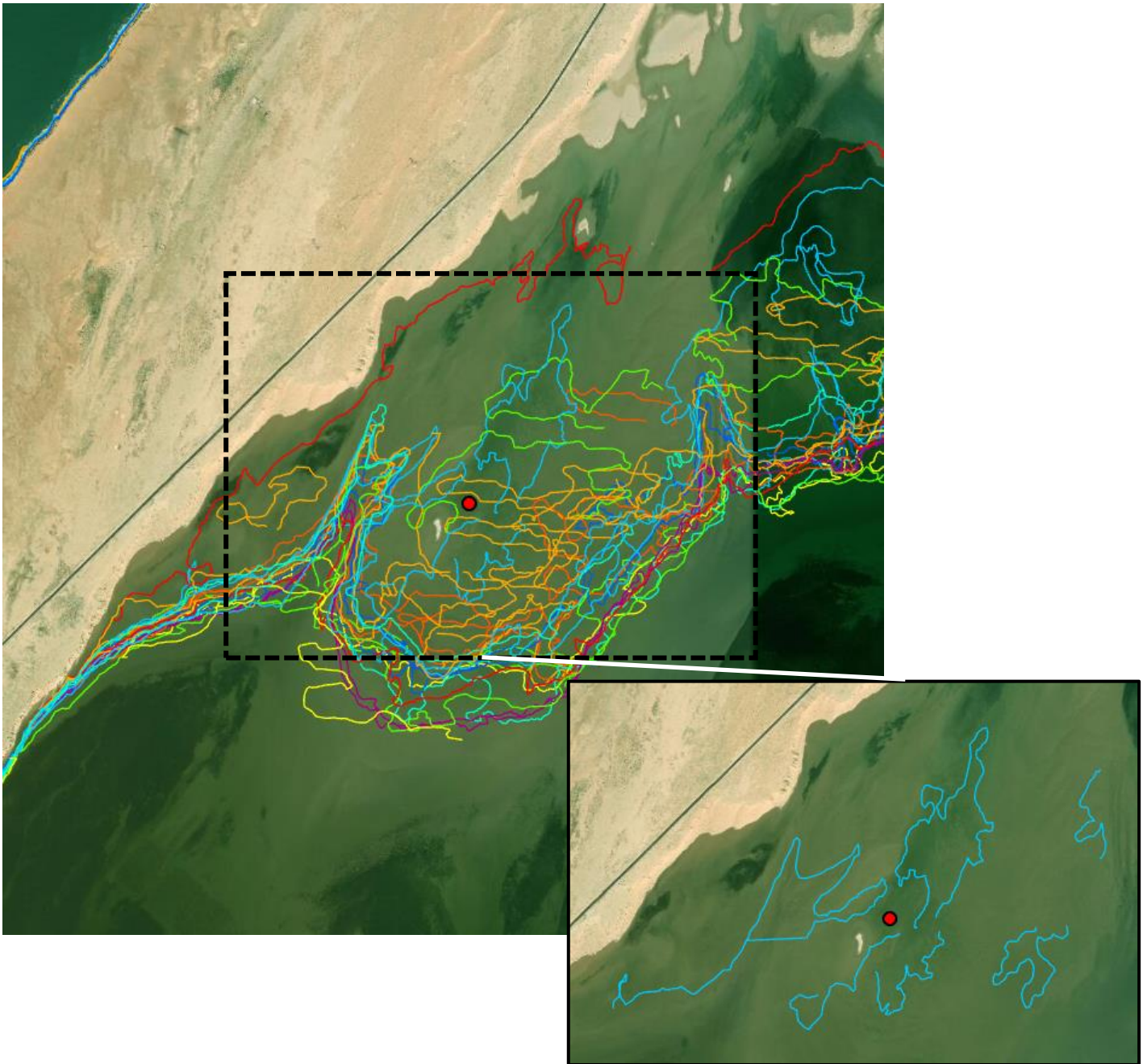


Figure iv. Shorelines mapped in the Dakhla Bay, Morocco on the Atlantic coast. Very low topography and high tidal influence means that calculating change rates is difficult even when using median composite images. Inset = Shoreline at 2015 and point feature indicating the mean centre point of all the 2015 shorelines. Basemap source: ArcGIS Basemap (2013) - Esri, DigitalGlobe, GeoEye, i-cubed, USDA FSA, USGS, AEX, Getmapping, Aerogrid, IGN, IGP, swisstopo, and the GIS User Community)

## Annex B Shoreline Change Rates / Admin Level 2 (Governorate/Province)

Admin Level 1	Admin Level 2	Change Rate (m/yr.) (Luijendijk et al, 2018)	Change Rate (m/yr.)	Confidence interval (m/yr. @ 95%)	Standard Error (m)	Number of Intersecting shorelines
<b>Tunisia</b>						
Ariana	Kalaat El Andalous	-10.73	-1.13	1.61	16.42	17.50
Ariana	Raoued	1.18	1.09	0.63	7.89	19.05
Beja	Nefza	-0.44	0.75	0.94	12.23	19.44
Ben Arous (Tunis Sud)	Ezzahra	0.90	1.19	0.48	6.05	19.13
Ben Arous (Tunis Sud)	Hammam Chott	0.03	-0.05	0.51	6.45	19.57
Ben Arous (Tunis Sud)	Hammam Lif	0.49	0.45	0.72	9.14	19.52
Ben Arous (Tunis Sud)	Rades	-2.85	0.30	0.95	11.07	18.07
Bizerte	Bizerte Nord	0.53	0.35	0.73	9.53	20.00
Bizerte	Bizerte Sud	-0.10	0.11	0.87	10.92	19.99
Bizerte	Ghar El Melh	-2.08	0.08	0.90	11.39	19.69
Bizerte	Menzel Bourguiba	N/A	-0.68	0.73	9.18	19.31
Bizerte	Menzel Jemil	-0.11	-0.15	0.66	8.66	20.00
Bizerte	Ras Jebel	-0.47	-0.44	0.63	8.28	20.00
Bizerte	Sejnane	0.65	-0.16	0.82	10.62	20.00
Bizerte	Tinja	N/A	0.66	0.94	11.82	18.51
Bizerte	Utique	-6.01	-2.67	3.03	33.77	16.94
Gabes	Gabes Medina	0.47	2.32	0.80	9.32	15.43
Gabes	Gabes Sud	-4.00	-1.14	0.44	5.07	13.43
Gabes	Ghannouch	-1.32	0.36	0.71	8.98	19.95
Gabes	Mareth	-2.96	2.38	3.05	27.66	14.46
Gabes	Metouia	-1.96	0.09	0.75	9.35	19.29
Jendouba	Tabarka	1.37	0.27	0.74	9.37	19.58
Mahdia	Chebba	-0.97	0.53	0.90	10.86	20.00
Mahdia	Ksour Essef	-0.12	-0.12	0.35	4.63	20.00
Mahdia	Mahdia	-0.34	-0.09	0.60	7.78	20.00
Mahdia	Melloulech	-1.50	0.15	0.43	5.74	20.00
Médenine	Ben Guerdane	-0.95	-0.98	0.79	7.39	18.76
Médenine	Djerba Ajim	-1.18	0.46	4.38	4.36	5.00
Médenine	Djerba Midoun	-1.14	0.88	4.46	4.43	5.00

Admin Level 1	Admin Level 2	Change Rate (m/yr.) (Luijendijk et al, 2018)	Change Rate (m/yr.)	Confidence interval (m/yr. @ 95%)	Standard Error (m)	Number of Intersecting shorelines
Médenine	Houmt Souk	0.04	0.52	4.96	4.93	5.00
Médenine	Médenine Sud	0.05	-0.97	1.80	17.71	18.58
Médenine	Sidi Makhlouf	3.55	-0.07	0.63	8.07	20.00
Médenine	Zarzis	0.69	0.11	1.11	11.69	18.51
Monastir	Bekalta	2.18	-0.16	0.53	6.88	20.00
Monastir	Ksibet El Mediouni	0.18	1.08	0.64	8.47	20.00
Monastir	Monastir	-0.40	0.30	0.73	8.80	18.74
Monastir	Sayada-Lamta-Bou Hjar	0.69	1.24	0.98	11.91	19.26
Monastir	Teboulba	0.08	1.21	0.67	8.81	20.00
Nabeul	Beni Khiar	-0.03	-0.06	0.81	10.54	20.00
Nabeul	Dar Chaabane El Fehri	N/A	0.65	0.72	9.26	20.00
Nabeul	El Mida	1.57	-0.61	0.96	8.89	12.36
Nabeul	Grombalia	0.41	0.85	0.42	5.30	19.88
Nabeul	Hammam Ghezaz	-0.11	-0.41	0.94	11.86	19.06
Nabeul	Hammamet	1.02	0.98	0.80	10.33	20.00
Nabeul	Haouaria	-0.75	-0.10	0.94	10.68	17.94
Nabeul	Kelibia	1.18	-0.51	0.66	8.40	19.54
Nabeul	Korba	-2.05	-2.02	1.31	16.26	18.49
Nabeul	Menzel Temime	0.25	0.05	1.40	17.40	18.98
Nabeul	Nabeul	-0.48	0.89	1.00	13.01	20.00
Nabeul	Soliman	-0.99	0.33	0.86	10.85	19.49
Nabeul	Takelsa	-0.54	-0.49	0.74	9.45	19.33
Sfax	Agareb	-0.31	1.01	0.76	10.05	20.00
Sfax	El Amra	-0.03	0.85	0.91	11.79	20.00
Sfax	El Ghraiba	-4.13	-0.05	5.70	45.45	12.37
Sfax	Jebeniana	-0.85	0.41	0.53	6.75	20.00
Sfax	Kerkennah	-0.50	-0.25	0.68	8.46	20.00
Sfax	Mahres	0.04	0.21	1.03	11.73	19.65
Sfax	Sakiet Eddaier	6.52	1.05	0.83	9.24	19.77
Sfax	Sfax Medina	10.93	N/A	N/A	N/A	N/A
Sfax	Sfax Sud	1.67	0.83	0.81	10.28	19.85
Sfax	Skhira	-4.38	0.05	0.89	10.82	19.58
Sousse	Akouda	-3.62	0.13	0.64	8.24	19.58
Sousse	Bouficha	-0.02	0.13	0.63	8.00	20.00



Admin Level 1	Admin Level 2	Change Rate (m/yr.) (Luijendijk et al, 2018)	Change Rate (m/yr.)	Confidence interval (m/yr. @ 95%)	Standard Error (m)	Number of Intersecting shorelines
Sousse	Enfidha	-0.30	-0.27	0.49	6.34	20.00
Sousse	Hammam Sousse	-0.47	-0.84	0.70	9.12	20.00
Sousse	Hergla	-1.44	0.34	0.85	11.13	20.00
Sousse	Sidi Bou Ali	-2.03	N/A	N/A	N/A	N/A
Sousse	Sousse Medina	-0.81	-0.48	0.64	8.00	18.95
Tunis	Carthage	0.23	-0.66	1.04	11.23	17.61
Tunis	La Goulette	0.50	-1.02	1.06	13.00	18.11
Tunis	La Marsa	-0.19	-0.22	0.65	8.44	20.00
<b>Western Sahara</b>						
	Tarfaya*	-0.24	-1.01	1.34	11.86	13.89
	Boujdour	0.10	-0.46	0.89	10.35	17.49
	Laayoune	-0.07	-0.34	0.66	7.67	17.69
	Oued el Dahab	-0.14	-0.36	1.06	10.76	16.99
<b>Morocco</b>						
Casablanca Settats	Berrechid Province	-0.4	-0.03	1.02	12.09	19.30
Casablanca Settats	El Jadida Province	-0.3	-0.58	1.14	13.24	18.47
Casablanca Settats	Nouaceur Province	0.33	0.28	1.12	11.91	16.81
Casablanca Settats	Prefecture of Casablanca	0.28	1.27	1.41	15.71	18.27
Casablanca Settats	Prefecture of Mohammedia	0.1	0.23	1.05	12.45	19.05
Casablanca Settats	Province de Benslimane	-0.43	1.12	1.77	17.25	17.16
Casablanca Settats	Province de Sidi Bennour	0.13	-0.07	0.77	8.34	18.11
Guelmim Noun	Oued Guelmim Province	0.49	0.37	1.65	16.78	13.24
Guelmim Noun	Oued Province de Tan Tan	-0.02	-0.56	1.07	12.37	17.80
Guelmim Noun	Oued Sidi Ifni Province	-0.22	-0.21	1.01	11.3	16.02
Marrakech Safi	Essaouira Province	-0.66	-0.56	1.17	14.07	19.21
Marrakech Safi	Province de Safi	-0.22	-0.46	0.79	9.53	19.64
Oriental	Province de Berkane	-1.16	-0.17	1.51	17.62	19.79
Oriental	Province de Driouch	0.1	-0.48	0.94	11.41	19.61

Admin Level 1	Admin Level 2	Change Rate (m/yr.) (Luijendijk et al, 2018)	Change Rate (m/yr.)	Confidence interval (m/yr. @ 95%)	Standard Error (m)	Number of Intersecting shorelines
Oriental	Province de Nador	-0.06	-0.19	0.88	10.42	19.10
Rabat Sale Kenitra	Prefecture de Skhirate Temara	-0.06	0.11	0.72	8.36	18.34
Rabat Sale Kenitra	Prefecture of Rabat	1.34	-0.39	0.85	8.05	16.29
Rabat Sale Kenitra	Prefecture of Sale	0.29	0.46	0.85	10.28	18.74
Rabat Sale Kenitra	Province de Kenitra	0.14	0.12	1.06	12.71	19.55
Souss Massa	Agadir Ida Outanane Prefecture	-0.36	0.29	1.07	12.56	18.05
Souss Massa	Chtouka Ait Baha Province	-0.59	0.33	1.09	12.6	17.52
Souss Massa	Inezgane Ait Melloul Prefecture	-2.15	-1.99	1.38	16.32	18.11
Souss Massa	Tiznit Province	-0.48	0.03	1.1	12.89	17.41
Tangier Tetouan Al Hoceima	Al Hoceima Province	0.33	-0.94	1.71	17	18.25
Tangier Tetouan Al Hoceima	Chefchaouen Province	-0.61	0.89	1.71	14.89	14.69
Tangier Tetouan Al Hoceima	Fahs Anjra Province	2.49	1.9	2.21	17.09	15.07
Tangier Tetouan Al Hoceima	Larache Province	0.03	-0.42	0.99	11.41	18.31
Tangier Tetouan Al Hoceima	Prefecture de M diq Fnideq	-0.53	0.7	0.74	8.15	17.70
Tangier Tetouan Al Hoceima	Prefecture of Tangier Assilah	-0.39	0.32	1.34	16.29	19.72
Tangier Tetouan Al Hoceima	Tetouan Province	-0.23	1.11	0.89	9.92	17.86

\*Admin region not included in Humanitarian Data file

Standard Error = Average distance (m) for each point from the regression line calculated for each transect. The standard error of the estimate assesses the accuracy of the best-fit regression line in predicting the position of a shoreline for a given point in time